

# RoboStream: Weaving Spatio-Temporal Reasoning with Memory in Vision-Language Models for Robotics

Yuzhi Huang<sup>1,2\*†♣</sup> Jie Wu<sup>1,2\*†</sup> Weijue Bu<sup>3</sup> Ziyi Xiong<sup>2,4‡</sup> Gaoyang Jiang<sup>5</sup> Ye Li<sup>1,2‡</sup>  
Kangye Ji<sup>1,2‡</sup> Shuzhao Xie<sup>1</sup> Yue Huang<sup>6</sup> Chenglei Wu<sup>2</sup> Jingyan Jiang<sup>4†</sup> Zhi Wang<sup>1†</sup>

<sup>1</sup> Shenzhen International Graduate School, Tsinghua University

<sup>2</sup> YXGN Robotics

<sup>3</sup> China University of Mining and Technology

<sup>4</sup> Shenzhen Technology University

<sup>5</sup> Huazhong University of Science and Technology

<sup>6</sup> Xiamen University

Website: <https://robostream123.github.io/>

**Abstract.** Enabling reliable long-horizon robotic manipulation is a crucial step toward open-world embodied intelligence. However, VLM-based planners treat each step as an isolated observation-to-action mapping, forcing them to reinfer scene geometry from raw pixels at every decision step while remaining unaware of how prior actions have reshaped the environment. Despite strong short-horizon performance, these systems lack the spatio-temporal reasoning required for persistent geometric anchoring and memory of action-triggered state transitions. Without persistent state tracking, perceptual errors accumulate across the execution horizon, temporarily occluded objects are catastrophically forgotten, and these compounding failures lead to precondition violations that cascade through subsequent steps. In contrast, humans maintain a persistent mental model that continuously tracks spatial relations and action consequences across interactions rather than reconstructing them at each instant. Inspired by this human capacity for causal spatio-temporal reasoning with persistent memory, we propose **RoboStream**, a training-free framework that achieves geometric anchoring through Spatio-Temporal Fusion Tokens (STF-Tokens), which bind visual evidence to 3D geometric attributes for persistent object grounding, and maintains causal continuity via a Causal Spatio-Temporal Graph (CSTG) that records action-triggered state transitions across steps. This design enables the planner to trace causal chains and preserve object permanence under occlusion without additional training or fine-tuning. RoboStream achieves 90.5% on long-horizon RL Bench and 44.4% on challenging real-world block-building tasks, where both SoFar and VoxPoser score 11.1%, demonstrating that spatio-temporal reasoning and causal memory are critical missing components for reliable long-horizon manipulation.

**Keywords:** Robot Manipulation · Vision-Language Models · Long-Horizon Planning · Spatio-Temporal Reasoning · Causal Memory

---

\* Equal contribution. † Corresponding author. ♣ Project lead.

‡ Work done during an internship at YXGN Robotics.

## 1 Introduction

Vision-language models (VLMs) have emerged as powerful planners for robotic manipulation, leveraging internet-scale semantic knowledge and visual perception to translate high-level instructions into executable action sequences [14, 30, 32, 73]. VLM-based systems have demonstrated strong performance on short-horizon manipulation tasks, including precise grasping, pose-aware placement, and decomposition of language instructions into subgoal sequences [4, 25, 41, 49].

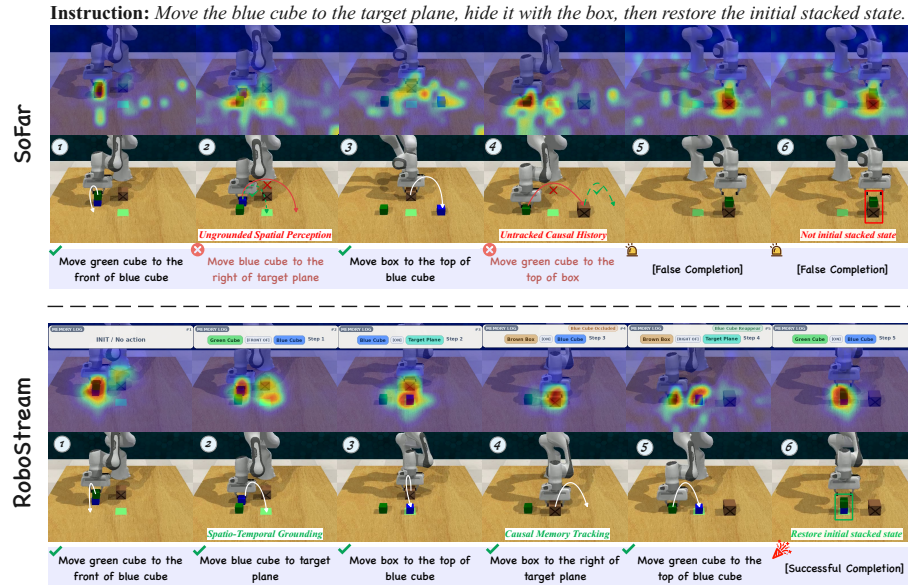


**Fig. 1: Qualitative comparison between SoFar [41] and RoboStream.** This long-horizon task involves object occlusion and state restoration. **Top (SoFar):** Diffuse attention heatmaps and absent memory logs reveal two cascading failures: *Ungrounded Spatial Perception* misplaces the blue cube at Step 2, while *Untracked Causal History* leaves the planner unaware of the occluded cube at Step 4, resulting in an incorrect final state. **Bottom (RoboStream):** Concentrated attention heatmaps and persistent memory logs show that *Spatio-Temporal Grounding* enables accurate object placement at Step 2, while *Causal Memory Tracking* maintains awareness of the occluded cube at Step 4, enabling successful task completion.

However, this success does not readily extend to long-horizon tasks, which demand sustained spatial and causal awareness across multi-step action sequences that irreversibly alter the environment [48, 58, 68]. Current VLM-based planners lack the persistent state tracking required to bridge observations across steps, forcing them to reinfer world state from partial observations at each decision step [18, 27, 71]. Without accumulated context, perceptual errors and action effects

compound across steps, ultimately resulting in cascading failures, as illustrated in Fig. 1. In contrast, humans maintain a coherent mental model [33] that continuously integrates spatial relations and causal consequences as actions unfold, tracking not only where objects are but also how each action has cumulatively reshaped the world.

Replicating this human capacity for spatio-temporal reasoning requires persistent tracking of two interdependent quantities, namely the evolving geometric state of each object across steps and the causal record of how actions modify those states. Tracking alone is insufficient, as geometric states must be anchored in 3D space for reliable spatial reasoning while causal records must be structured to support inference over displaced or occluded objects. Current VLM-based planners fail at both, as illustrated in Fig. 1, exposing two tightly coupled representation deficits. ① *Ungrounded Spatial Perception*: spatial relations in manipulation are latent state components continually rewritten by contact and motion, yet current systems infer them implicitly via image-centric perception without geometric anchoring or cross-step identity binding [8, 21, 64]. This forces geometry reconstruction from raw pixels at every step, where small inaccuracies accumulate into spatial hallucinations and precondition violations. ② *Untracked Causal History*: although actions irreversibly alter the environment, existing methods retain no record linking actions to induced state transitions. Without causal tracking, planners remain unaware of displaced objects and lose track of occluded ones entirely, leading to precondition violations when subsequent actions depend on altered states [57, 69].

To address these two deficits, we propose **RoboStream**, a training-free framework that weaves spatio-temporal reasoning and persistent memory directly into the VLM planning loop through *Spatio-Temporal Grounding* and *Causal Memory Tracking*. For grounding, Spatio-Temporal Fusion Tokens (STF-Tokens) distill visual appearance and 3D geometry (centroid and Gaussian shape) of each object into identity-persistent primitives, shifting VLM reasoning from pixel-level reconstruction to structured object-instance references that suppress cascading spatial errors. For tracking, a Causal Spatio-Temporal Graph (CSTG) records action-triggered state transitions alongside persistent object identities, preserving object permanence under occlusion without direct visual evidence. We evaluate RoboStream on five benchmarks spanning simulated and real-world settings: SIMPLER [35], long-horizon RL Bench tasks [29], 6-DoF SpatialBench [41], Open6DOR V2 [12], and long-horizon real-world Franka experiments including block building, disassembly, and hide-and-restore under occlusion. Across all settings, RoboStream outperforms existing VLM-based planners, demonstrating that spatio-temporal reasoning and persistent memory are essential for robust long-horizon manipulation. Our contributions are as follows:

- 1) We introduce **RoboStream**, a training-free framework weaving spatio-temporal reasoning with persistent memory to overcome spatial hallucination and causal blindness in VLM-based planners. By anchoring geometric evidence across steps and tracking causal state transitions, RoboStream builds persistent world representations enabling robust long-horizon reasoning without retraining.

2) We design two synergistic mechanisms for Spatio-Temporal Grounding and Causal Memory Tracking. *Spatio-Temporal Fusion Tokens (STF-Tokens)* bind visual evidence to 3D geometry, converting pixel-level inference into deterministic spatial references. A *Causal Spatio-Temporal Graph (CSTG)* maintains object identities and records action-triggered state transitions, enabling causal inference of occluded states and preventing error accumulation over long horizons.

3) RoboStream achieves state-of-the-art results across five benchmarks spanning long-horizon manipulation (RLBench, real-world Franka), zero-shot generalization (SIMPLER), and spatial reasoning (6-DoF SpatialBench, Open6DOR V2), validating that weaving spatio-temporal reasoning with persistent memory is essential for robust manipulation across diverse settings.

## 2 Related Work

### 2.1 Spatial Understanding with VLMs

Spatial understanding underpins robotic manipulation by recovering geometric relationships. Approaches overcome VLM limitations through two main strategies. Tool-augmented methods [12, 42, 52, 72] delegate VLMs to orchestrate external visual foundation models or geometric engines. SpaceTools [9] combines dual-interaction reinforcement learning with geometric reasoning, while TIGER [19] synthesizes code-based geometric routines. These externalize computation but add overhead and require module coupling. 3D-data-driven fine-tuning [10, 11, 45, 51, 55] strengthens spatial representations through pseudo-3D or real-world 3D data. RoboRefer [70] integrates depth encoders, SpatialBot [5] applies progressive spatial curricula, and SpatialVLM [8] leverages large-scale 3D spatial QA datasets. Fine-tuning incurs substantial data and training costs. RoboStream contrasts by anchoring visual evidence directly to explicit 3D geometry via STF-Tokens, requiring no fine-tuning and maintaining persistent spatial representations across sequential steps without external modules or retraining.

### 2.2 VLMs for Robotic Manipulation

Robotic manipulation bridges semantic reasoning with execution along three complementary axes. Logic-grounded task planning [23, 26, 50, 66] decomposes instructions into structured sequences. SayCan [4] scores action feasibility via affordance models, while Code as Policies [37] synthesizes executable programs for long-horizon scheduling. These methods prioritize logical structure but treat execution steps independently. Geometry-aware constraint generation [16, 22, 24, 46, 63, 64] grounds planning in spatial constraints. VoxPoser [25] synthesizes 3D value maps for zero-shot planning, CoPa [21] defines constraints over geometric keypoints, and SoFar [41] maps language to 6-DoF poses. However, these approaches reconstruct geometric constraints at each step without persistent tracking. Closed-loop reasoning [14, 15, 38, 71] enhances adaptability through perceptual feedback. Inner Monologue [27] implements self-correcting loops, and VILA [20] reasons over

image sequences for physical intuition. Yet these methods remain reactive, recovering from failures without reasoning about action-induced state changes or preconditions. RoboStream unifies geometry and causality through a CSTG that records action-state transitions, enabling VLMs to maintain causal consistency while reasoning about occluded states and external disturbances.

### 2.3 Long-Horizon Task Planning

Long-horizon manipulation poses a distinct challenge, requiring systems to translate high-level instructions into coherent action sequences while maintaining consistency across extended temporal spans. Dynamic visual conditions and partial observability amplify this challenge regarding causal consistency across sequential decisions [18]. Hierarchical decomposition [2, 36, 47] organizes multi-step execution by encoding intermediate representations. HiRobot [48] segments instructions into atomic commands, DexVLA [57] couples VLM planning with diffusion-based policies, and RoboMatrix [39] implements three-tier hierarchical control. LoHoVLA [62] aligns semantic intent via natural-language sub-goals. These strategies organize execution without tracking how past actions reshape the environment. Chain-of-thought methods [40, 56, 65, 67] strengthen planning via explicit future-state reasoning. CoT-VLA [68] reasons over latent visual subgoals, ManualVLA [17] generates executable visual guidance, and GR-3 [7] learns flow-matching trajectories. While improving short-horizon decisions, these methods lack persistent memory to track action consequences. RoboStream addresses this gap through a CSTG recording actions, environmental consequences, and external disturbances, enabling VLMs to trace state evolution and reason causally about how past actions constrain future possibilities under partial observability.

## 3 Method

### 3.1 Overview

VLMs exhibit strong generalization in high-level manipulation planning [4, 32, 73], yet existing planners treat each step independently, lacking the persistent spatio-temporal memory required for long-horizon tasks. Without structured world-state tracking, perception errors compound over time and recovery from unexpected disturbances becomes intractable. We propose RoboStream, which constructs geometry-grounded STF-Tokens by binding visual evidence to 3D geometric attributes from RGB-D observations (Sec. 3.3), organizes them into a Causal Spatio-Temporal Graph (CSTG) that maintains persistent object identities and logs action-triggered state transitions in a sliding-window memory (Sec. 3.4), and feeds this structured memory into the VLM for chain-of-thought verification to generate 6-DoF action directives (Sec. 3.5), as illustrated in Fig. 2.

Formally, given RGB-D observation  $(I_t, D_t)$ , goal specification  $I_{\text{goal}}$ , and memory  $\mathcal{M}_{<t}$ , RoboStream constructs STF-Tokens encoding per-object 3D geometric properties and visual appearance:

$$\mathcal{T}_t^{\text{STF}} = \Phi_{\text{enc}}(I_t, D_t \mid \mathcal{M}_{<t}), \quad (1)$$

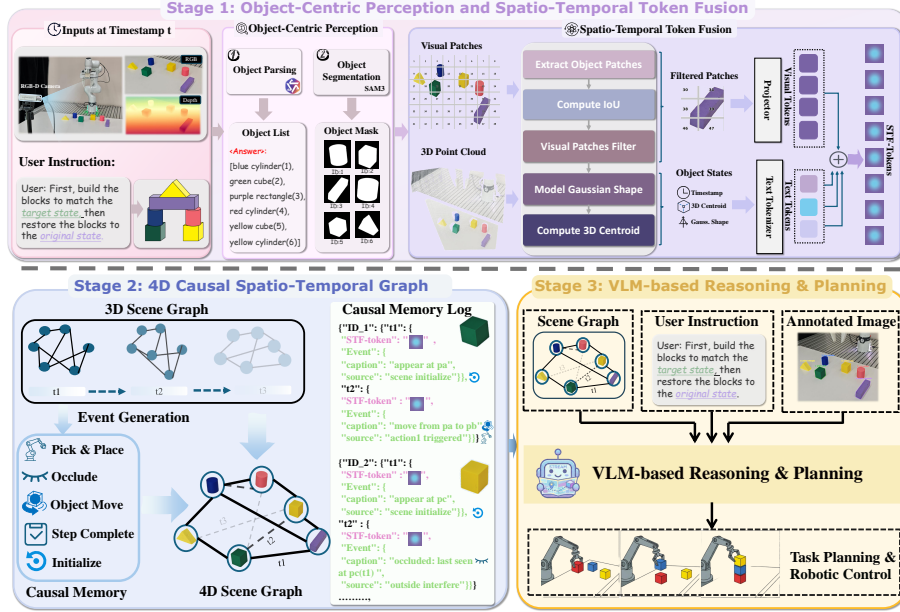


**Fig. 2: Overview of the RoboStream Framework.** The system processes multi-modal RGB-D inputs through three hierarchical stages: (1) Object-Centric Perception and Spatio-Temporal Token Fusion, where raw visual data is distilled into STF-Tokens by grounding visual evidence within 3D geometric primitives (centroids and Gaussian shapes); (2) 4D Causal Spatio-Temporal Graph Construction, which maintains persistent memory encoding object identities and state transitions across time steps; and (3) VLM-based Reasoning and Planning, where the VLM leverages both the CSTG and visual inputs to perform high-level task planning and precise robotic manipulation.

which are incorporated as nodes into the CSTG  $\mathcal{G}_t^{\text{CST}}$ . By recursively merging incoming STF-Tokens with historical graph state, the CSTG maintains persistent object identities and inter-object spatial relations across time without requiring model retraining:

$$\mathcal{G}_t^{\text{CST}} = \Psi_{\text{graph}}(\mathcal{T}_t^{\text{STF}}, \mathcal{G}_{t-1}^{\text{CST}}). \quad (2)$$

Action generation is then decoupled to balance VLM semantic generalization with robot execution precision. Given a context-augmented prompt  $\mathcal{P}_t$  assembled from  $\mathcal{G}_t^{\text{CST}}$  and the current observation, the VLM produces a semantic action directive  $\hat{a}_t$  conditioned on the goal  $I_{\text{goal}}$  and the accumulated causal history:

$$\hat{a}_t = \Pi_{\theta}(I_{\text{goal}}, \mathcal{P}_t | \mathcal{G}_t^{\text{CST}}), \quad (3)$$

which is deterministically instantiated into a 6-DoF pose by resolving object identities against the geometry of STF-Tokens stored in  $\mathcal{G}_t^{\text{CST}}$ :

$$a_t = \Phi_{\text{inst}}(\hat{a}_t, \mathcal{G}_t^{\text{CST}}). \quad (4)$$

This decoupled design preserves VLM semantic reasoning while delegating precise coordinate extraction to deterministic geometry resolution, enabling training-free deployment across various scenarios. We elaborate on each stage in Sec. 3.3–3.5.

### 3.2 Object-Centric Perception

To construct scene representations prioritizing task-relevant entities, we employ a two-stage perception pipeline. Given the RGB-D observation  $(I_t, D_t)$ , goal specification  $I_{\text{goal}}$ , and accumulated memory  $\mathcal{M}_{<t}$ , we prompt a VLM to identify task-relevant objects and output open-vocabulary descriptors  $\mathcal{D} = \{d_1, \dots, d_N\}$  [41,70]. The goal specification  $I_{\text{goal}}$  accepts either a reference goal image or a natural language instruction, both applicable in real-world and simulation settings. Conditioning on  $\mathcal{M}_{<t}$  allows the descriptor set to maintain consistent object identities across steps, implicitly filtering task-irrelevant entities and reducing computational overhead in downstream modules. The resulting descriptors condition an open-vocabulary segmentation model to produce pixel-accurate masks  $\{M_i\}_{i=1}^N = \text{SAM3}(I_t, \mathcal{D})$  [6], where  $M_i \in \{0, 1\}^{H \times W}$ . Combined with the depth map  $D_t$  [61], each mask defines a spatially coherent region for 3D point cloud extraction, providing the inputs to  $\Phi_{\text{enc}}$  for constructing  $\mathcal{T}_t^{\text{STF}}$  as in Sec. 3.3.

### 3.3 Spatio-Temporal Token Fusion

Given instance masks  $\{M_i\}_{i=1}^N$  and the point cloud from the perception stage, we construct a per-object Spatio-Temporal Fusion Token  $\tau_i^t$  by integrating visual evidence with metric geometry into a unified, object-centric representation; the full set  $\mathcal{T}_t^{\text{STF}} = \{\tau_i^t\}_{i=1}^N$  constitutes the encoder output  $\Phi_{\text{enc}}$  defined in Sec. 3.1. For each object  $o_i$ , the mask  $M_i$  is applied to the RGB observation  $I_t$  to obtain a masked image  $\hat{I}_i^t$ , which is passed through the VLM visual encoder [13,44] to produce a  $16 \times 16$  grid of patch tokens. Patches with an IoU exceeding  $I_{th}$  relative to  $M_i$  are selected, projected into the language space, and aggregated to form the visual evidence  $\mathbf{v}_i^t$ . Unlike methods that pass multiple masked images directly to the VLM, this design avoids redundant background processing by compressing each object’s filtered visual tokens, spatial position, geometry, and temporal trajectory into a compact token sequence, shifting VLM reasoning from raw pixels to structured object instances.

In parallel, we define a shape representation vector  $\mathbf{s}_i^t$  constructed from Gaussian distribution parameters and geometric extrema along each spatial axis:  $\mathbf{s}_i^t = \{(\mu_a, \sigma_a, a_{\min}, a_{\max}) \mid a \in \{x, y, z\}\}$ . Unlike traditional bounding boxes, this captures geometric extent more completely, with the joint mean-standard-deviation encoding suppressing outlier noise while correcting Gaussian approximation bias. The centroid  $\mathbf{c}_i^t = \text{median}(\mathbf{P}_i) \in \mathbb{R}^3$  is extracted from the object-specific point cloud  $\mathbf{P}_i$ . Both  $\mathbf{c}_i^t$  and  $\mathbf{s}_i^t$  are serialized via the text tokenizer into the same language embedding space as  $\mathbf{v}_i^t$ , placing visual appearance and 3D geometry within a single context window. This shared space allows the VLM to jointly attend over heterogeneous visual and spatial signals without architectural

modification, encoding the complete per-object state as:

$$\tau_i^t = \langle \mathbf{v}_i^t, \mathbf{c}_i^t, \mathbf{s}_i^t, t \rangle, \quad (5)$$

where  $t$  denotes the current timestamp. By grounding visual tokens in explicit 3D geometry and temporal context, STF-Tokens enable deterministic spatial queries and suppress cascading errors in long-horizon manipulation tasks.

### 3.4 4D Causal Spatio-Temporal Graph

While STF-Tokens stabilize per-object spatial perception, long-horizon manipulation additionally requires reasoning about inter-object spatial relations and action causality. We address this by constructing the Causal Spatio-Temporal Graph (CSTG)  $\mathcal{G}_t^{\text{CST}}$  [1, 54], which realizes the graph update operator  $\Psi_{\text{graph}}$  in Sec. 3.1 by integrating incoming STF-Tokens  $\mathcal{T}_t^{\text{STF}}$  with the historical state  $\mathcal{G}_{t-1}^{\text{CST}}$  through a spatial scene graph and a causal memory log. At each timestamp  $t$ , we construct a spatial scene graph  $\mathcal{G}_t = (\mathcal{V}_t, \mathcal{E}_t)$  where each node  $v_i \in \mathcal{V}_t$  corresponds to an object in  $\mathcal{T}_t^{\text{STF}}$  and maintains a sliding-window buffer  $\{\tau_i^{t-K+1}, \dots, \tau_i^t\}$  of length  $K$ . Edges  $e_{ij} \in \mathcal{E}_t$  encode pairwise spatial relations via Euclidean distance  $d_{ij} = \|\mathbf{c}_i - \mathbf{c}_j\|_2$  and directional offset  $\Delta \mathbf{c}_{ij} = \mathbf{c}_j - \mathbf{c}_i$ .

Building upon this structure, semantic events are detected by comparing STF-Tokens across the sliding window, covering both object-level events (e.g., planned displacement, unintended collision, occlusion) and task-level events (e.g., action execution, subtask completion). Each event is recorded with its timestamp, location, and causal source in the memory log  $\mathcal{H}_t^K$ , which is integrated with the spatial graph to form the complete CSTG:

$$\mathcal{G}_t^{\text{CST}} = (\mathcal{G}_t, \mathcal{H}_t^K). \quad (6)$$

This structured representation enables deterministic verification of action pre-conditions at each planning step, triggering re-planning upon detected failure to prevent error accumulation over long horizons.

### 3.5 VLM-based Causal Reasoning and Planning

At each planning step, RoboStream assembles the context-augmented prompt  $\mathcal{P}_t$  from the CSTG  $\mathcal{G}_t^{\text{CST}}$  encoding current object states and spatial relations, the annotated observation with object identity labels overlaid [60], and the goal specification  $I_{\text{goal}}$ . This fusion of structured causal memory with grounded visual evidence enables  $H_\theta$  to reason jointly over historical context and current scene geometry. The VLM then performs chain-of-thought spatial verification [56], reviewing historical states, checking action pre-conditions against object geometry, and resolving causal conflicts from occlusion or dependencies, before generating the semantic action directive  $\hat{a}_t$  as defined in Eq. 3. Finally,  $\hat{a}_t$  is instantiated into the 6-DoF action  $a_t$  via  $\Phi_{\text{inst}}$  by resolving object identities against STF-Token geometry stored in  $\mathcal{G}_t^{\text{CST}}$  (Sec. 3.1).

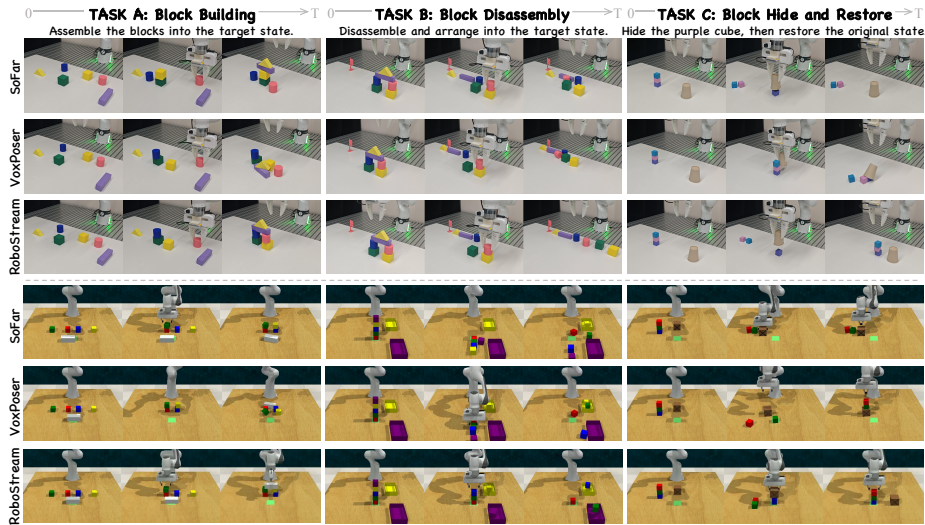


**Fig. 3: Qualitative results in real-world and simulated manipulation tasks.** We evaluate on three challenging tasks: (a) Block Building, demanding precise bottom-to-top assembly toward a target configuration; (b) Block Disassembly, requiring structured top-to-bottom deconstruction and rearrangement; and (c) Block Hide and Restore, requiring causal memory maintenance under full occlusion. RoboStream consistently outperforms SoFar [41] and VoxPoser [25], particularly in spatio-temporal perception and causal memory over extended horizons.

## 4 Experiments

### 4.1 Experimental Setup

We evaluate RoboStream across five benchmarks spanning physical and simulated environments, covering real-world manipulation on a Franka Research 3 arm (Sec. 4.2), long-horizon tasks on RL Bench [29] (Sec. 4.4), zero-shot generalization on SIMPLER [35] (Sec. 4.3), and 6-DoF spatial reasoning on SpatialBench [41] and Open6DOR V2 [12] (Sec. 4.5). Short-horizon evaluation validates that the geometry grounding of STF-Tokens suppresses spatial hallucination in individual actions; long-horizon evaluation tests whether the full framework sustains causal state tracking and correct action ordering. We instantiate RoboStream with three VLM backbones, Qwen3-VL-8B, Qwen3-VL-32B, and Qwen3-VL-235B [59], hereafter referred to as RoboStream-8B, RoboStream-32B, and RoboStream-235B respectively. All variants operate in a manner without environment-specific adaptation or fine-tuning across any benchmark. We compare against state-of-the-art baselines including SoFar [41], VoxPoser [25], and RT-2-X [73], measuring execution success rate for manipulation tasks and accuracy for spatial reasoning.

To accommodate task diversity, we adopt two goal-specification strategies. For real-world experiments and RL Bench long-horizon tasks, where target configurations are difficult to fully capture in text, we employ image-guided goal

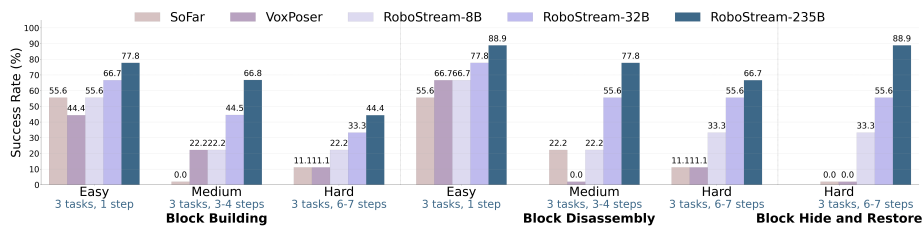


**Fig. 4: Performance comparison on zero-shot real-world manipulation tasks.** We design 21 diverse tasks covering block building (Task A), block disassembly (Task B), and block hide and restore (Task C).

specification with images depicting the desired final state, such as blocks arranged in a target tower configuration. For SIMPLER short-horizon tasks, and tasks involving occlusion or state restoration, we employ text-guided natural language instructions, such as “hide the blue cube, then restore the original state.”

## 4.2 Real-World Robotic Manipulation

**Tasks and Evaluations.** We construct 21 real-world tasks on a Franka Research 3 (FR3) arm equipped with a parallel gripper and a front-view Intel RealSense D435i RGB-D camera, utilizing 17 colored objects, as shown in Fig. 3. The tasks are categorized into three types evaluating different cognitive and physical reasoning dimensions. Task A (Block Building) assesses spatio-temporal grounding and pre-condition adherence by stacking objects Bottom-to-Top across three difficulty levels (Easy, Medium, Hard), requiring the robot to verify base stability before proceeding. Task B (Block Disassembly) evaluates sequential state tracking and support relation maintenance during Top-to-Bottom removal, requiring accurate causal memory of stacking order and support dependencies. Task C (Block Hide and Restore) stress-tests causal memory and object permanence under full occlusion, where the robot must conceal a block beneath a cup, execute distractor steps, and restore the original configuration by retrieving object identity and last known pose from causal history. Tasks A and B are specified by goal images, while Task C is guided by natural language instructions. Each task is executed three times, with details in the Appendix.

**Results.** As shown in Fig. 4, all RoboStream variants consistently outperform baselines across all difficulty levels, with success rates scaling proportionally with backbone capacity. On Hard-level block building and disassembly tasks, RoboStream-235B achieves success rates of 44.4% and 66.7%, respectively. In contrast, prior reactive systems such as SoFar [41] and VoxPoser [25] exhibit limited efficacy, struggling to exceed 11.1% without persistent causal tracking and physical state evolution awareness. In Task C (Block Hide and Restore), requiring accurate tracking under total occlusion, RoboStream-235B achieves 88.9% while even our lightweight 8B variant maintains 33.3%, whereas SoFar and VoxPoser completely fail at 0%. This contrast highlights that structured spatio-temporal

**Table 1: Quantitative success rate comparison on the SIMPLER benchmark.** We evaluate: (a) the Google Robot setup under Variant Aggregation (VA) and Visual Matching (VM) protocols, and (b) the WidowX + Bridge setup. For the WidowX tasks, we use the following abbreviations: Spoon (Put Spoon on Towel), Carrot (Put Carrot on Plate), Stack (Stack Green Block on Yellow Block), and Egg (Put Eggplant in Basket). “Zero” in the Data column indicates zero-shot evaluation.

(a) Google Robot Setup				(b) WidowX + Bridge Setup						
Set	Policy	Pick	Coke Move Near	Policy	Data	Spoon	Carrot	Stack	Egg	Avg
VA	RT-1-X [3]	49.0	32.3	RT-1-X [3]	OXE	0.0	4.2	0.0	0.0	1.1
	RT-2-X [73]	82.3	79.2	Octo-B [53]	OXE	12.5	8.3	0.0	43.1	16.0
	Octo-B [53]	0.6	3.1	Octo-S [53]	OXE	47.2	9.7	4.2	56.9	30.0
	OpenVLA [32]	54.5	47.7	OpenVLA [32]	OXE	0.0	0.0	0.0	4.1	1.0
	SoFar [41]	90.7	74.0	RoboVLM [34]	OXE	20.8	25.0	8.3	0.0	13.5
	<b>RoboStream-8B</b>	<b>94.2</b>	<b>79.8</b>	RoboVLM [34]	Bridge	29.2	25.0	12.5	58.3	31.3
VM	RT-1-X [3]	56.7	31.7	SpatialVLA [43]	OXE	20.8	20.8	25.0	70.8	34.4
	RT-2-X [73]	78.7	77.9	SpatialVLA [43]	Bridge	16.7	25.0	29.2	<b>100.0</b>	42.7
	Octo-B [53]	17.0	4.2	SoFar [41]	Zero	<u>58.3</u>	<u>66.7</u>	<u>70.8</u>	37.5	<u>58.3</u>
	OpenVLA [32]	16.3	46.2	<b>RoboStream-8B Zero</b>		<b>62.5</b>	<b>71.9</b>	<b>77.1</b>	<u>87.5</u>	<b>74.8</b>
	SoFar [41]	92.3	91.7							
	<b>RoboStream-8B</b>	<b>95.7</b>	<b>95.8</b>							

memory is far more decisive for hidden-state tasks than scaling reactive systems. The monotonic gains across model scales confirm that STF-Tokens and CSTG provide complementary capabilities growing increasingly effective with model capacity, yielding robustness that purely reactive systems cannot replicate.

### 4.3 Simulation Object Manipulation Evaluation on SIMPLER

We evaluate zero-shot cross-embodiment generalization on the SIMPLER benchmark [35] across Google Robot and WidowX + Bridge configurations, representing substantial domain shifts from training environments. These short-horizon tasks isolate STF-Token contributions by testing whether spatial grounding transfers across embodiments and viewpoints, independent of long-horizon reasoning.

**Google Robot Configuration.** As shown in Tab. 1, RoboStream-8B achieves superior success rates on both “Pick Coke Can” and the spatially demanding “Move Near” tasks under VM evaluation, surpassing the prior state-of-the-art SoFar [41]. Notably, RoboStream-8B also outperforms OXE-finetuned RT-2-X [73] by a substantial margin despite operating fully zero-shot. Under the more challenging VA evaluation, RoboStream-8B maintains competitive performance, again exceeding SoFar. Consistent gains across both protocols and tasks with varying geometry confirm stable spatial grounding independent of embodiment.

**WidowX + Bridge Configuration.** RoboStream achieves a higher average success rate across all subtasks compared to zero-shot SoFar and Bridge-finetuned SpatialVLA [43] without requiring any fine-tuning or domain adaptation. Notably, this advantage holds despite SpatialVLA being explicitly trained on in-domain Bridge data, highlighting the superior transferability of our geometry-grounded representation. These results confirm that spatio-temporal reasoning grounded in

**Table 2: Simulation evaluation of long-horizon manipulation on RL Bench.** All RoboStream variants are evaluated in a zero-shot manner without in-domain fine-tuning.

Tasks	SoFar [41]	VoxPoser [25]	RoboStream-8B	RoboStream-32B	RoboStream-235B
Bridge Between Towers	52.0	8.0	76.0	88.0	88.0
Cover Top Block with Box	4.0	4.0	40.0	84.0	92.0
Cover Bottom Block with Box	0.0	0.0	16.0	68.0	96.0
Place Blocks in Two Containers	100.0	96.0	100.0	100.0	100.0
Place Blocks in Two Cont. (Hard)	4.0	4.0	24.0	76.0	88.0
Stack Five Colors	4.0	4.0	60.0	72.0	80.0
Stack Three Colors	60.0	96.0	96.0	96.0	96.0
Unstack then Stack Four Colors	0.0	0.0	52.0	76.0	84.0
<b>Average</b>	28.0	26.5	58.0	82.5	90.5

explicit geometric primitives transfers robustly across embodiments and extends naturally from short tasks to subsequent long-horizon benchmarks.

#### 4.4 Simulation Long-Horizon Task Evaluation on RL Bench

**Tasks and Evaluations.** To assess long-horizon manipulation capabilities, we introduce 8 complex tasks within RL Bench [29] (Tab. 2), constructed by extending and reconfiguring native assets. Each method is evaluated over 25 episodes per task using different random seeds. Following Sec. 4.1, tasks are categorized by guidance modality. Five goal-image-guided tasks require visually complex target configurations, including Bridge Between Towers, Place Blocks in Two Containers, Place Blocks in Two Cont. (Hard), and Stack Three/Five Colors. Three text-guided tasks stress-test action ordering, restoration, and object permanence under occlusion, including Cover Top/Bottom Block with Box and Unstack then Stack Four Colors. Detailed setups are provided in the Appendix.

**Results.** As shown in Tab. 2, RoboStream consistently outperforms both SoFar [41] and VoxPoser [25] across these long-horizon scenarios. Notably, our framework demonstrates a strong scaling effect, with performance increasing alongside model capacity to reach a 90.5% average success rate on RoboStream-235B without additional training, as larger capacity provides the reasoning depth necessary to maintain logical consistency over extended action sequences. However, scaling the VLM alone is not a panacea for long-horizon stability. Even our smallest variant, RoboStream-8B, substantially exceeds much larger baselines, demonstrating that spatio-temporal reasoning and structured memory are more critical for physical consistency than simply increasing parameter scale.

#### 4.5 6-DoF Spatial Reasoning Evaluation

To evaluate how STF-Tokens bridge high-level visual features with precise instance-level 3D grounding, we extend our evaluation to rotation and full 6-DoF pose estimation. Following SoFar [41], we incorporate PointSO for 6-DoF prediction and evaluate on Open6DOR V2 [12] and 6-DoF SpatialBench [41]. Since SoFar serves as our primary baseline, we include variants using Qwen3-VL-8B and Qwen3-VL-32B backbones for fair cross-scale comparison with RoboStream.

**Table 3: Spatial reasoning evaluation on 6-DoF SpatialBench [41].** Results are categorized by spatial VQA task types, covering absolute (*abs.*) and relative (*rel.*) reasoning for both position and orientation.

Method	Position		Orientation		Total
	rel.	abs.	rel.	abs.	
GPT-4o [28]	49.4	28.4	44.2	25.8	36.2
SpaceMantis [8]	33.6	29.2	27.2	25.0	28.9
RoboPoint [64]	43.8	30.8	33.8	25.8	33.5
SoFar [41]	59.6	33.8	<b>54.6</b>	31.3	43.9
SoFar-8B [41]	41.5	24.3	27.1	31.3	30.5
SoFar-32B [41]	<u>60.4</u>	<u>41.9</u>	45.8	33.3	<u>45.3</u>
<b>RoboStream-8B</b>	47.2	31.1	35.4	<u>35.4</u>	36.8
<b>RoboStream-32B</b>	<b>66.0</b>	<b>44.6</b>	<u>48.0</u>	<b>37.5</b>	<b>48.9</b>

**Table 4: 6-DoF object rearrangement evaluation on Open6DOR [12].** Results are categorized by position (*Pos.*), rotation (*Rot.*), and integrated 6-DoF success rates.

Method	Pos.	Rot.	6-DoF
Dream2Real [31]	15.9	31.3	13.5
VoxPoser [25]	32.6	-	-
Open6DOR-GPT [12]	74.9	41.1	35.6
SoFar [41]	93.0	<u>57.0</u>	<u>48.7</u>
SoFar-8B [41]	92.4	42.9	45.1
SoFar-32B [41]	<u>93.1</u>	54.6	48.4
<b>RoboStream-8B</b>	<u>93.1</u>	47.6	47.3
<b>RoboStream-32B</b>	<b>93.8</b>	<b>58.8</b>	<b>52.2</b>

**Table 5: Ablation study on RoboStream-235B.** Success rates (%) across 8 long-horizon tasks, isolating contributions of CSTG and STF-Tokens.

<i>STF-Tokens</i>	<i>CSTG</i>	Bridge Between Towers	Cover Top Block	Cover Bottom Block	Place in Containers	Place in Containers (Hard)	Stack Five Colors	Stack Three Colors	Unstack then Stack	Average
✗	✗	0.0	0.0	0.0	84.0	12.0	0.0	0.0	0.0	12.0
✓	✗	0.0	0.0	0.0	<u>92.0</u>	24.0	0.0	0.0	0.0	14.5
✗	✓	<u>72.0</u>	<u>84.0</u>	<u>88.0</u>	<b>100.0</b>	<u>72.0</u>	<u>60.0</u>	<b>96.0</b>	<u>64.0</u>	<u>79.5</u>
✓	✓	<b>88.0</b>	<b>92.0</b>	<b>96.0</b>	<b>100.0</b>	<b>88.0</b>	<b>80.0</b>	<b>96.0</b>	<b>84.0</b>	<b>90.5</b>

**Spatial Reasoning on 6-DoF SpatialBench.** As shown in Tab. 3, RoboStream-32B achieves superior overall performance, outperforming both SoFar and GPT-4o [28]. The most pronounced gains appear on absolute and relative position tasks, where pure image-text alignment is most susceptible to spatial ambiguity. These results confirm that the core advantage of STF-Tokens lies not in coordinate injection alone, but in serving as a geometric anchor providing deterministic spatial reference when visual features and language descriptions conflict.

**6-DoF Object Rearrangement on Open6DOR V2.** As shown in Tab. 4, RoboStream-32B consistently outperforms SoFar across position, rotation, and integrated 6-DoF metrics. Unlike baselines treating spatial coordinates as text annotations, STF-Tokens distill per-object visual evidence into structured instance representations encoding centroid, Gaussian shape, and orientation. This shift from pixel-level to object-level reasoning underlies consistent gains across all tracks, most notably on 6-DoF where tight placement constraints demand precise geometric grounding and spatial alignment.

#### 4.6 Ablation Study

We ablate RoboStream-235B across all 8 long-horizon RL Bench [29] tasks to isolate the contribution of each architectural component (Tab. 5). Removing the CSTG module (*w/o CSTG*) causes the average success rate to collapse from 90.5% to 14.5%, confirming that persistent state tracking is the foundational

driver for long-horizon tasks. However, while CSTG provides logical structure, STF-Tokens provide physical precision. Removing STF-Tokens (*w/o STF-Tokens*) results in an 11.0% absolute drop (from 90.5% to 79.5%), demonstrating that without explicit 3D geometric grounding, even a CSTG-equipped agent struggles with compounding spatial inaccuracies during contact-rich execution. The mutual dependence of both components becomes evident when removing them simultaneously (*w/o Both*), which yields only 12.0% success rate. Notably, comparing this to the *w/o CSTG* variant (14.5%) shows that STF-Tokens still provide marginal improvement in short-horizon spatial accuracy even when long-horizon logic fails. Their full potential, however, is unlocked only when coupled with the CSTG, where CSTG ensures correct action sequencing and STF-Tokens ensure each step is executed with deterministic spatial precision.

## 5 Conclusion

RoboStream addresses two representation deficits that cause VLM-based planners to fail on long-horizon manipulation. The first is Ungrounded Spatial Perception, where geometry from raw pixels allows small inaccuracies to compound into spatial hallucinations. The second is Untracked Causal History, where absent action-state records leave planners unaware of displaced or occluded objects. STF-Tokens resolve the first via Spatio-Temporal Grounding by distilling per-object appearance and 3D geometry into identity-persistent primitives. The CSTG resolves the second via Causal Memory Tracking by maintaining persistent records of state transitions, enabling inference of hidden object states. Across five benchmarks including RLBench, SIMPLER, SpatialBench, Open6DOR V2, and real-world Franka experiments, RoboStream consistently outperforms existing methods, establishing that weaving spatio-temporal reasoning with persistent memory is more decisive for long-horizon stability than model scale alone.

## 6 Limitation

As a decoupled planning-execution framework, RoboStream shares a limitation inherent to the broader VLM-for-robotics paradigm. Imperfections in any submodule, including unstable grasping or perceptual uncertainty, can propagate into execution failures even when high-level planning is correct. This reflects a fundamental tension between semantic generalization of VLM-based planners and physical precision demanded by low-level control, a challenge broadly applicable to decoupled systems beyond RoboStream. Future work includes exploring hybrid approaches that bridge VLM planner generalization with end-to-end execution fluency, either by adopting a Vision-Language-Action (VLA) model as the downstream controller for smoother and more compliant motion, or by developing a fully end-to-end VLA that internalizes spatio-temporal reasoning and causal memory within the action generation loop. Extending RoboStream to contact-rich, dexterous, and open-world manipulation also constitutes a promising direction.

## References

1. Armeni, I., He, Z.Y., Gwak, J., Zamir, A.R., Fischer, M., Malik, J., Savarese, S.: 3d scene graph: A structure for unified semantics, 3d space, and camera. In: Proceedings of the IEEE/CVF international conference on computer vision. pp. 5664–5673 (2019)
2. Belkhale, S., Ding, T., Xiao, T., Sermanet, P., Vuong, Q., Tompson, J., Chebotar, Y., Dwibedi, D., Sadigh, D.: Rt-h: Action hierarchies using language. arXiv preprint arXiv:2403.01823 (2024)
3. Brohan, A., Brown, N., Carbajal, J., Chebotar, Y., Dabis, J., Finn, C., Gopalakrishnan, K., Hausman, K., Herzog, A., Hsu, J., et al.: Rt-1: Robotics transformer for real-world control at scale. arXiv preprint arXiv:2212.06817 (2022)
4. Brohan, A., Chebotar, Y., Finn, C., Hausman, K., Herzog, A., Ho, D., Ibarz, J., Irpan, A., Jang, E., Julian, R., et al.: Do as i can, not as i say: Grounding language in robotic affordances. In: Conference on robot learning. pp. 287–318. PMLR (2023)
5. Cai, W., Ponomarenko, I., Yuan, J., Li, X., Yang, W., Dong, H., Zhao, B.: Spatialbot: Precise spatial understanding with vision language models. In: 2025 IEEE International Conference on Robotics and Automation (ICRA). pp. 9490–9498. IEEE (2025)
6. Carion, N., Gustafson, L., Hu, Y.T., Debnath, S., Hu, R., Suris, D., Ryali, C., Alwala, K.V., Khedr, H., Huang, A., et al.: Sam 3: Segment anything with concepts. arXiv preprint arXiv:2511.16719 (2025)
7. Cheang, C., Chen, S., Cui, Z., Hu, Y., Huang, L., Kong, T., Li, H., Li, Y., Liu, Y., Ma, X., et al.: Gr-3 technical report. arXiv preprint arXiv:2507.15493 (2025)
8. Chen, B., Xu, Z., Kirmani, S., Ichter, B., Sadigh, D., Guibas, L., Xia, F.: Spatialvlm: Endowing vision-language models with spatial reasoning capabilities. In: Proceedings of the IEEE/CVF Conference on Computer Vision and Pattern Recognition. pp. 14455–14465 (2024)
9. Chen, S., Uy, M.A., Song, C.H., Ladhak, F., Murali, A., Qu, Q., Birchfield, S., Blukis, V., Tremblay, J.: Spacetools: Tool-augmented spatial reasoning via double interactive rl. arXiv preprint arXiv:2512.04069 (2025)
10. Cheng, A.C., Yin, H., Fu, Y., Guo, Q., Yang, R., Kautz, J., Wang, X., Liu, S.: Spatialrgpt: Grounded spatial reasoning in vision-language models. Advances in Neural Information Processing Systems **37**, 135062–135093 (2024)
11. Daxberger, E., Wenzel, N., Griffiths, D., Gang, H., Lazarow, J., Kohavi, G., Kang, K., Eichner, M., Yang, Y., Dehghan, A., et al.: Mm-spatial: Exploring 3d spatial understanding in multimodal llms. In: Proceedings of the IEEE/CVF International Conference on Computer Vision. pp. 7395–7408 (2025)
12. Ding, Y., Geng, H., Xu, C., Fang, X., Zhang, J., Wei, S., Dai, Q., Zhang, Z., Wang, H.: Open6dor: Benchmarking open-instruction 6-dof object rearrangement and a vlm-based approach. In: 2024 IEEE/RSJ International Conference on Intelligent Robots and Systems (IROS). pp. 7359–7366. IEEE (2024)
13. Dosovitskiy, A., Beyer, L., Kolesnikov, A., Weissenborn, D., Zhai, X., Unterthiner, T., Dehghani, M., Minderer, M., Heigold, G., Gelly, S., et al.: An image is worth 16x16 words: Transformers for image recognition at scale. arXiv preprint arXiv:2010.11929 (2020)
14. Driess, D., Xia, F., Sajjadi, M.S., Lynch, C., Chowdhery, A., Ichter, B., Wahid, A., Tompson, J., Vuong, Q., Yu, T., et al.: Palm-e: An embodied multimodal language model. In: International Conference on Machine Learning. pp. 8469–8488. PMLR (2023)

15. Du, Y., Konyushkova, K., Denil, M., Raju, A., Landon, J., Hill, F., de Freitas, N., Cabi, S.: Vision-language models as success detectors. arXiv preprint arXiv:2303.07280 (2023)
16. Fang, K., Liu, F., Abbeel, P., Levine, S.: Moka: Open-world robotic manipulation through mark-based visual prompting. Robotics: Science and Systems XX (2024)
17. Gu, C., Liu, J., Chen, H., Huang, R., Wuwu, Q., Liu, Z., Li, X., Li, Y., Zhang, R., Jia, P., et al.: Manualvla: A unified vla model for chain-of-thought manual generation and robotic manipulation. arXiv preprint arXiv:2512.02013 (2025)
18. Han, S., Qiu, B., Liao, Y., Huang, S., Gao, C., YAN, S., Liu, S.: Robocerebra: A large-scale benchmark for long-horizon robotic manipulation evaluation. In: The Thirty-ninth Annual Conference on Neural Information Processing Systems Datasets and Benchmarks Track
19. Han, Y., Chi, C., Zhou, E., Rong, S., An, J., Wang, P., Wang, Z., Sheng, L., Zhang, S.: Tiger: Tool-integrated geometric reasoning in vision-language models for robotics. arXiv preprint arXiv:2510.07181 (2025)
20. Hu, Y., Lin, F., Zhang, T., Yi, L., Gao, Y.: Look before you leap: Unveiling the power of gpt-4v in robotic vision-language planning. In: First Workshop on Vision-Language Models for Navigation and Manipulation at ICRA 2024
21. Huang, H., Lin, F., Hu, Y., Wang, S., Gao, Y.: Copa: General robotic manipulation through spatial constraints of parts with foundation models. In: 2024 IEEE/RSJ International Conference on Intelligent Robots and Systems (IROS). pp. 9488–9495. IEEE (2024)
22. Huang, S., Chang, H., Liu, Y., Zhu, Y., Dong, H., Boularias, A., Gao, P., Li, H.: A3vlm: Actionable articulation-aware vision language model. In: Conference on Robot Learning. pp. 1675–1690. PMLR (2025)
23. Huang, W., Abbeel, P., Pathak, D., Mordatch, I.: Language models as zero-shot planners: Extracting actionable knowledge for embodied agents. In: International conference on machine learning. pp. 9118–9147. PMLR (2022)
24. Huang, W., Wang, C., Li, Y., Zhang, R., Fei-Fei, L.: Rekep: Spatio-temporal reasoning of relational keypoint constraints for robotic manipulation. In: Conference on Robot Learning. pp. 4573–4602. PMLR (2025)
25. Huang, W., Wang, C., Zhang, R., Li, Y., Wu, J., Fei-Fei, L.: Voxposer: Composable 3d value maps for robotic manipulation with language models. In: Conference on Robot Learning. pp. 540–562. PMLR (2023)
26. Huang, W., Xia, F., Shah, D., Driess, D., Zeng, A., Lu, Y., Florence, P., Mordatch, I., Levine, S., Hausman, K., et al.: Grounded decoding: Guiding text generation with grounded models for embodied agents. *Advances in Neural Information Processing Systems* **36**, 59636–59661 (2023)
27. Huang, W., Xia, F., Xiao, T., Chan, H., Liang, J., Florence, P., Zeng, A., Tompson, J., Mordatch, I., Chebotar, Y., et al.: Inner monologue: Embodied reasoning through planning with language models. In: Conference on Robot Learning. pp. 1769–1782. PMLR (2023)
28. Hurst, A., Lerer, A., Goucher, A.P., Perelman, A., Ramesh, A., Clark, A., Ostrow, A., Welihinda, A., Hayes, A., Radford, A., et al.: Gpt-4o system card. arXiv preprint arXiv:2410.21276 (2024)
29. James, S., Ma, Z., Arrojo, D.R., Davison, A.J.: Rlbench: The robot learning benchmark & learning environment. *IEEE Robotics and Automation Letters* **5**(2), 3019–3026 (2020)
30. Jiang, Y., Gupta, A., Zhang, Z., Wang, G., Dou, Y., Chen, Y., Fei-Fei, L., Anandkumar, A., Zhu, Y., Fan, L.: Vima: Robot manipulation with multimodal prompts. In: International Conference on Machine Learning. pp. 14975–15022. PMLR (2023)

31. Kapelyukh, I., Ren, Y., Alzugaray, I., Johns, E.: Dream2Real: Zero-shot 3D object rearrangement with vision-language models. In: 2024 IEEE International Conference on Robotics and Automation (ICRA). pp. 4796–4803. IEEE (2024)
32. Kim, M.J., Pertsch, K., Karamcheti, S., Xiao, T., Balakrishna, A., Nair, S., Rafailov, R., Foster, E.P., Sanketi, P.R., Vuong, Q., et al.: Openvla: An open-source vision-language-action model. In: Conference on Robot Learning. pp. 2679–2713. PMLR (2025)
33. Lake, B.M., Ullman, T.D., Tenenbaum, J.B., Gershman, S.J.: Building machines that learn and think like people. *Behavioral and brain sciences* **40**, e253 (2017)
34. Li, X., Li, P., Qian, L., Liu, M., Wang, D., Liu, J., Kang, B., Ma, X., Wang, X., Guo, D., et al.: What matters in building vision–language–action models for generalist robots. *Nature Machine Intelligence* pp. 1–15 (2026)
35. Li, X., Hsu, K., Gu, J., Mees, O., Pertsch, K., Walke, H.R., Fu, C., Lunawat, I., Sieh, I., Kirmani, S., et al.: Evaluating real-world robot manipulation policies in simulation. In: Conference on Robot Learning. pp. 3705–3728. PMLR (2025)
36. Li, Y., Deng, Y., Zhang, J., Jang, J., Memmel, M., Garrett, C.R., Ramos, F., Fox, D., Li, A., Gupta, A., et al.: Hamster: Hierarchical action models for open-world robot manipulation. In: The Thirteenth International Conference on Learning Representations
37. Liang, J., Huang, W., Xia, F., Xu, P., Hausman, K., Ichter, B., Florence, P., Zeng, A.: Code as policies: Language model programs for embodied control. In: 2023 IEEE International conference on robotics and automation (ICRA). pp. 9493–9500. IEEE (2023)
38. Liu, H., Chen, A., Zhu, Y., Swaminathan, A., Kolobov, A., Cheng, C.A.: Interactive robot learning from verbal correction. In: 2nd Workshop on Language and Robot Learning: Language as Grounding
39. Mao, W., Zhong, W., Jiang, Z., Fang, D., Zhang, Z., Lan, Z., Li, H., Jia, F., Wang, T., Fan, H., et al.: Robomatrix: A skill-centric hierarchical framework for scalable robot task planning and execution in open-world. arXiv preprint arXiv:2412.00171 (2024)
40. Mu, Y., Zhang, Q., Hu, M., Wang, W., Ding, M., Jin, J., Wang, B., Dai, J., Qiao, Y., Luo, P.: Embodiedgpt: Vision-language pre-training via embodied chain of thought. *Advances in Neural Information Processing Systems* **36**, 25081–25094 (2023)
41. Qi, Z., Zhang, W., Ding, Y., Dong, R., Yu, X., Li, J., Xu, L., Li, B., He, X., Fan, G., et al.: Sofar: Language-grounded orientation bridges spatial reasoning and object manipulation. In: The Thirty-ninth Annual Conference on Neural Information Processing Systems
42. Qin, Y., Kang, L., Song, X., Yin, Z., Liu, X., Liu, X., Zhang, R., Bai, L.: Robofactory: Exploring embodied agent collaboration with compositional constraints. In: Proceedings of the IEEE/CVF International Conference on Computer Vision. pp. 10075–10085 (2025)
43. Qu, D., Song, H., Chen, Q., Yao, Y., Ye, X., Ding, Y., Wang, Z., Gu, J., Zhao, B., Wang, D., et al.: Spatialvla: Exploring spatial representations for visual-language-action model. arXiv preprint arXiv:2501.15830 (2025)
44. Radford, A., Kim, J.W., Hallacy, C., Ramesh, A., Goh, G., Agarwal, S., Sastry, G., Askell, A., Mishkin, P., Clark, J., et al.: Learning transferable visual models from natural language supervision. In: International conference on machine learning. pp. 8748–8763. PmLR (2021)
45. Ray, A., Duan, J., Brown II, E.L., Tan, R., Bashkirova, D., Hendrix, R., Ehsani, K., Kembhavi, A., Plummer, B.A., Krishna, R., et al.: Sat: Dynamic spatial aptitude

- training for multimodal language models. In: Second Conference on Language Modeling
46. Sharma, P., Sundaralingam, B., Blukis, V., Paxton, C., Hermans, T., Torralba, A., Andreas, J., Fox, D.: Correcting robot plans with natural language feedback. arXiv preprint arXiv:2204.05186 (2022)
  47. Shi, L., Hu, Z., Zhao, T., Sharma, A., Pertsch, K., Luo, J., Levine, S., Finn, C.: Yell at your robot: Improving on-the-fly from language corrections. *Robotics: Science and Systems XX* (2024)
  48. Shi, L.X., Ichter, B., Equi, M.R., Ke, L., Pertsch, K., Vuong, Q., Tanner, J., Walling, A., Wang, H., Fusai, N., et al.: Hi robot: Open-ended instruction following with hierarchical vision-language-action models. In: International Conference on Machine Learning. pp. 54919–54933. PMLR (2025)
  49. Shridhar, M., Manuelli, L., Fox, D.: Perceiver-actor: A multi-task transformer for robotic manipulation. In: Conference on Robot Learning. pp. 785–799. PMLR (2023)
  50. Singh, I., Blukis, V., Mousavian, A., Goyal, A., Xu, D., Tremblay, J., Fox, D., Thomason, J., Garg, A.: Progprompt: Generating situated robot task plans using large language models. In: 2023 IEEE International Conference on Robotics and Automation (ICRA). pp. 11523–11530. IEEE (2023)
  51. Song, C.H., Blukis, V., Tremblay, J., Tyree, S., Su, Y., Birchfield, S.: Robospacial: Teaching spatial understanding to 2d and 3d vision-language models for robotics. In: Proceedings of the Computer Vision and Pattern Recognition Conference. pp. 15768–15780 (2025)
  52. Tan, H., Hao, X., Chi, C., Lin, M., Lyu, Y., Cao, M., Liang, D., Chen, Z., Lyu, M., Peng, C., et al.: Roboos: A hierarchical embodied framework for cross-embodiment and multi-agent collaboration. arXiv preprint arXiv:2505.03673 (2025)
  53. Team, O.M., Ghosh, D., Walke, H., Pertsch, K., Black, K., Mees, O., Dasari, S., Hejna, J., Kreiman, T., Xu, C., et al.: Octo: An open-source generalist robot policy. arXiv preprint arXiv:2405.12213 (2024)
  54. Wald, J., Dhamo, H., Navab, N., Tombari, F.: Learning 3d semantic scene graphs from 3d indoor reconstructions. In: Proceedings of the IEEE/CVF Conference on Computer Vision and Pattern Recognition. pp. 3961–3970 (2020)
  55. Wang, X., Ma, W., Zhang, T., de Melo, C.M., Chen, J., Yuille, A.: Spatial457: A diagnostic benchmark for 6d spatial reasoning of large multimodal models. In: 2025 IEEE/CVF Conference on Computer Vision and Pattern Recognition (CVPR). pp. 24669–24679. IEEE (2025)
  56. Wei, J., Wang, X., Schuurmans, D., Bosma, M., Xia, F., Chi, E., Le, Q.V., Zhou, D., et al.: Chain-of-thought prompting elicits reasoning in large language models. *Advances in neural information processing systems* **35**, 24824–24837 (2022)
  57. Wen, J., Zhu, Y., Li, J., Tang, Z., Shen, C., Feng, F.: Dexvla: Vision-language model with plug-in diffusion expert for general robot control. In: Conference on Robot Learning. pp. 3094–3114. PMLR (2025)
  58. Wu, J., Antonova, R., Kan, A., Lepert, M., Zeng, A., Song, S., Bohg, J., Rusinkiewicz, S., Funkhouser, T.: Tidybot: Personalized robot assistance with large language models. In: 2023 IEEE/RSJ International Conference on Intelligent Robots and Systems (IROS). pp. 3546–3553. IEEE (2023)
  59. Yang, A., Li, A., Yang, B., Zhang, B., Hui, B., Zheng, B., Yu, B., Gao, C., Huang, C., Lv, C., et al.: Qwen3 technical report. arXiv preprint arXiv:2505.09388 (2025)
  60. Yang, J., Zhang, H., Li, F., Zou, X., Li, C., Gao, J.: Set-of-mark prompting unleashes extraordinary visual grounding in gpt-4v. arXiv preprint arXiv:2310.11441 (2023)

61. Yang, L., Kang, B., Huang, Z., Xu, X., Feng, J., Zhao, H.: Depth anything: Unleashing the power of large-scale unlabeled data. In: CVPR (2024)
62. Yang, Y., Sun, J., Kou, S., Wang, Y., Deng, Z.: Lohovla: A unified vision-language-action model for long-horizon embodied tasks. arXiv preprint arXiv:2506.00411 (2025)
63. Yu, W., Gileadi, N., Fu, C., Kirmani, S., Lee, K.H., Arenas, M.G., Chiang, H.T.L., Erez, T., Hasenclever, L., Humplik, J., et al.: Language to rewards for robotic skill synthesis. In: Conference on Robot Learning. pp. 374–404. PMLR (2023)
64. Yuan, W., Duan, J., Blukis, V., Pumacay, W., Krishna, R., Murali, A., Mousavian, A., Fox, D.: Robopoint: A vision-language model for spatial affordance prediction in robotics. In: Conference on Robot Learning. pp. 4005–4020. PMLR (2025)
65. Zawalski, M., Chen, W., Pertsch, K., Mees, O., Finn, C., Levine, S.: Robotic control via embodied chain-of-thought reasoning. In: Conference on Robot Learning. pp. 3157–3181. PMLR (2025)
66. Zeng, A., Attarian, M., Choromanski, K.M., Wong, A., Welker, S., Tombari, F., Purohit, A., Ryoo, M.S., Sindhvani, V., Lee, J., et al.: Socratic models: Composing zero-shot multimodal reasoning with language. In: The Eleventh International Conference on Learning Representations
67. Zhang, K., Yin, Z.H., Ye, W., Gao, Y.: Learning manipulation skills through robot chain-of-thought with sparse failure guidance. In: 2025 IEEE/RSJ International Conference on Intelligent Robots and Systems (IROS). pp. 8012–8018. IEEE (2025)
68. Zhao, Q., Lu, Y., Kim, M.J., Fu, Z., Zhang, Z., Wu, Y., Li, Z., Ma, Q., Han, S., Finn, C., et al.: Cot-vla: Visual chain-of-thought reasoning for vision-language-action models. In: Proceedings of the Computer Vision and Pattern Recognition Conference. pp. 1702–1713 (2025)
69. Zhen, H., Qiu, X., Chen, P., Yang, J., Yan, X., Du, Y., Hong, Y., Gan, C.: 3d-vla: A 3d vision-language-action generative world model. In: International Conference on Machine Learning. pp. 61229–61245. PMLR (2024)
70. Zhou, E., An, J., Chi, C., Han, Y., Rong, S., Zhang, C., Wang, P., Wang, Z., Huang, T., Sheng, L., et al.: Roborefer: Towards spatial referring with reasoning in vision-language models for robotics. In: The Thirty-ninth Annual Conference on Neural Information Processing Systems
71. Zhou, E., Su, Q., Chi, C., Zhang, Z., Wang, Z., Huang, T., Sheng, L., Wang, H.: Code-as-monitor: Constraint-aware visual programming for reactive and proactive robotic failure detection. In: Proceedings of the Computer Vision and Pattern Recognition Conference. pp. 6919–6929 (2025)
72. Zhu, K., Bai, F., Xiang, Y., Cai, Y., Chen, X., Li, R., Wang, X., Dong, H., Yang, Y., Fan, X., et al.: Dexflywheel: A scalable and self-improving data generation framework for dexterous manipulation. In: The Thirty-ninth Annual Conference on Neural Information Processing Systems
73. Zitkovich, B., Yu, T., Xu, S., Xu, P., Xiao, T., Xia, F., Wu, J., Wohlhart, P., Welker, S., Wahid, A., et al.: Rt-2: Vision-language-action models transfer web knowledge to robotic control. In: Conference on Robot Learning. pp. 2165–2183. PMLR (2023)

## Appendix

### A Robot Setups

#### A.1 Simulation Robot Setups

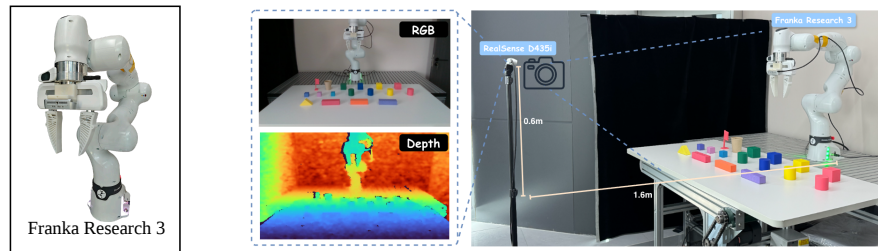
We run all simulation experiments in two benchmarks: RLBench [29] and SIMPLER [35].

(a) **RLBench setup.** We use the standard RLBench environment equipped with a Franka Emika Panda (7-DoF) arm and a Panda Gripper, utilizing a planning-based control stack. Our approach relies primarily on the front RGB-D camera as the main visual observation for planning. We report results on 15 short-horizon tasks and 8 long-horizon tasks.

(b) **SIMPLER setup.** We evaluate two embodiments in SIMPLER: Google Robot and WidowX + Bridge. For visual observations, we utilize the overhead camera for the Google Robot and the 3rd-view camera for WidowX. Crucially, we apply our training-free planning pipeline directly across both configurations without any environment-specific fine-tuning.

#### A.2 Real World Robot Setups

In our real-world experiments, we uniformly utilized a Franka Research 3 (FR3) robotic arm equipped with a parallel gripper. A front-view Intel RealSense D435i RGB-D camera was deployed to capture both visual and depth information for point cloud reconstruction. The detailed workspace and robot configurations are illustrated in Fig. 5.



(a) Franka Research 3.

(b) Workspace setup with RGB and depth views.

**Fig. 5: Real-world experimental setup.** (a) The Franka Research 3 robot arm used in our experiments. (b) The physical workspace equipped with the robot arm and an Intel RealSense D435i camera; the insets show the corresponding RGB view and depth map.

## B Experimental Assets and Task Design

**Real-World Experimental Assets.** As shown in Fig. 6, our real-world experiments utilize a diverse set of manipulation objects designed to evaluate precise

spatial reasoning and sequential stacking. These assets primarily consist of: (i) *Geometric primitives* including rectangular blocks, cubes, and cylinders in various sizes and distinct colors (pink, blue, green, yellow, purple, and orange); (ii) *A triangular prism* (yellow triangle in Fig. 6) used for assessing high-precision alignment and challenging placement tasks; and (iii) *Functional objects* (e.g., a pink flag and a brown cup) to create dynamic occlusion and nesting scenarios. In total, these 17 unique pieces allow for a vast combinatorial space of long-horizon tasks, such as multi-layer block building and disassembling, providing a rigorous testbed for the model’s object permanence and spatial consistency.

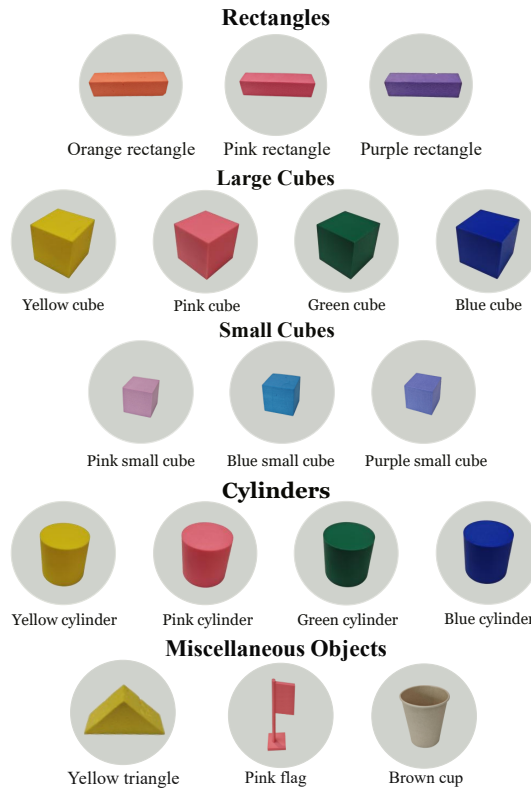


**Fig. 6: Assets for real-world experiments.** A collection of 17 manipulation objects including geometric primitives, a triangular prism, and functional objects used across all task difficulty levels.

### B.1 Design of Real World Tasks

To rigorously validate the core contributions of RoboStream, specifically the geometry-grounded perception of STF-Tokens and the causal state tracking of the CSTG, we engineered a hierarchical suite of 21 real-world tasks. Unlike

random pick-and-place scenarios, these tasks are hypothesis-driven stress tests designed to probe the boundaries of spatio-temporal reasoning. The evaluation is structured into three task categories (corresponding to Task A, B, and C in the main text), organized along two primary evaluation axes. (i) *Spatio-temporal grounding and sequential reasoning*: Tasks A (Block Building) and B (Block Disassembly) assess whether STF-Tokens and the CSTG sustain accurate spatial reasoning across progressively longer construction and deconstruction sequences, with target configurations specified by goal images. (ii) *Causal memory and object permanence*: Task C (Block Hide and Restore) stress-tests whether the CSTG preserves latent object states when visual evidence is entirely obliterated by occlusion, guided by natural language instructions. Each task configuration is executed three times.

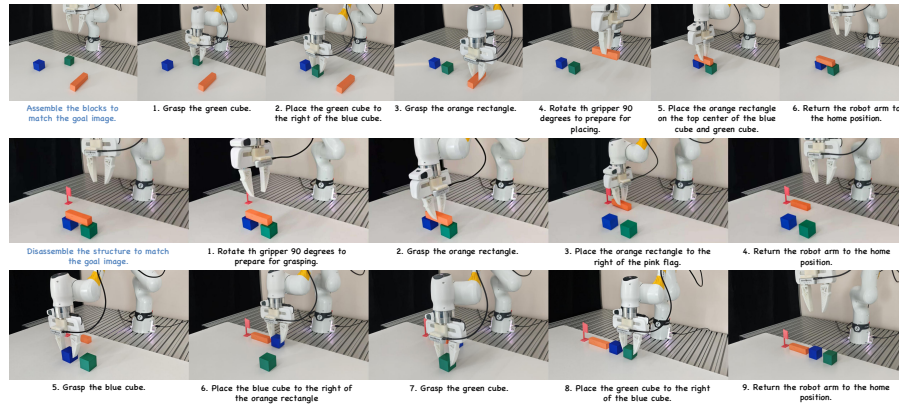


**Fig. 7: Long-horizon block manipulation (Easy).** Execution of basic assembly and disassembly involving 2–3 objects, demonstrating fundamental spatial grounding and pick-and-place precision.

**Block Building and Disassembly (Fig. 7, 8, 9).** These two categories jointly evaluate spatio-temporal grounding and sequential state tracking through symmetric construction and deconstruction sequences: Bottom-to-Top stacking (Block Building) and Top-to-Bottom removal (Block Disassembly), each across three synchronized difficulty levels. At the *Easy and Medium* levels, distractors sharing colors but differing in shape are deliberately introduced to test whether the model resists visual-semantic grounding errors; at each step the robot must verify base stability and placement pre-conditions before proceeding.

The *Hard* level scales to 7 objects and 6–7 sequential steps, imposing strict physical constraints from opposite directions. During building, the VLM must continuously update its scene representation via the CSTG, treating newly placed objects as valid geometric anchors for subsequent layers to suppress cascading spatial hallucinations. During disassembly, the model must instead deduce the

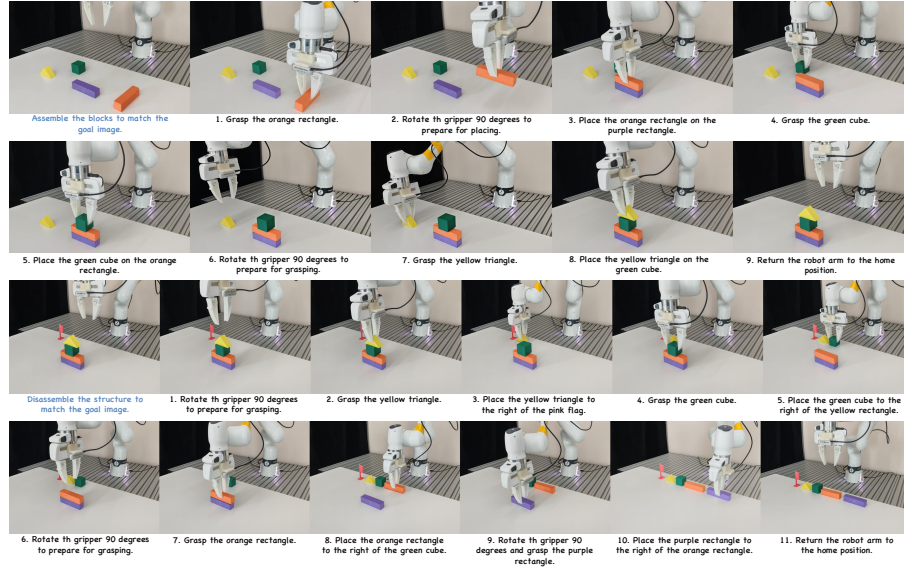


**Fig. 8: Long-horizon block manipulation (Medium).** Intermediate execution requiring a strict sequence of 3–4 steps to manipulate 4 objects, verifying sequential planning and state tracking.

correct Top-to-Bottom dependency chain from the CSTG; a single greedy mistake (such as extracting a bottom support block) causes immediate structural collapse, proving the necessity of explicit 3D structural reasoning and accurate causal memory of stacking order and support dependencies, which simple semantic matching cannot provide.

**Block Hide and Restore (Fig. 10).** To explicitly validate the necessity of the Causal Spatio-Temporal Graph (CSTG), we engineered Block Hide and Restore tasks that stress-test causal memory and object permanence under full occlusion. In the most challenging configuration, the robot is instructed to hide the *bottom* block of an existing tower. This forces a deep causal dependency chain: the model must autonomously deduce the physical necessity to first disassemble the blocking upper layers, conceal the target under an opaque cup, execute intermediate distractor steps, and ultimately reverse the entire sequence to restore the exact original tower.

This design creates an extreme perceptual bottleneck where direct visual evidence of the hidden object and its original stacking order is entirely obliterated. Successfully completing this task proves that RoboStream maintains a persistent causal spatio-temporal representation via the CSTG, relying on its causal memory log to track latent object identities and last-known poses when reactive visual perception fundamentally fails.

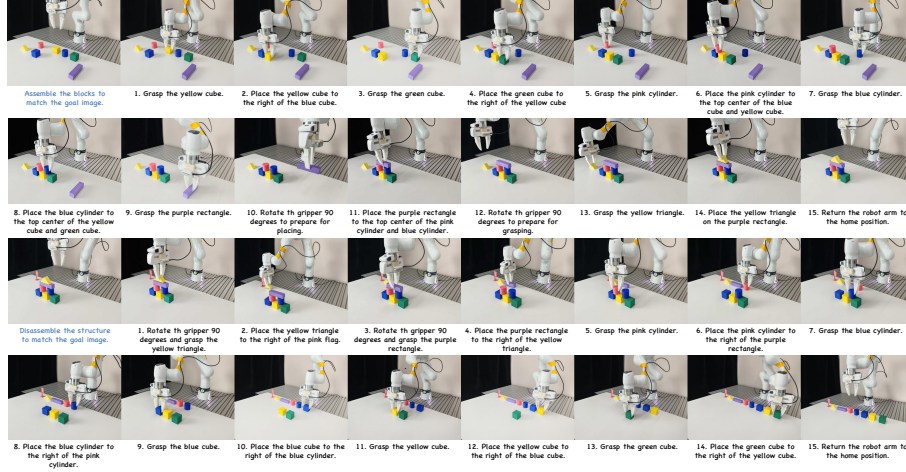


**Fig. 9: Long-horizon block manipulation (Hard).** Extreme long-horizon execution involving 7 objects and 6–7 steps. The sequence highlights the model’s ability to maintain physical stability during complex “Bottom-to-Top” building and “Top-to-Bottom” disassembly without collapsing the structure.

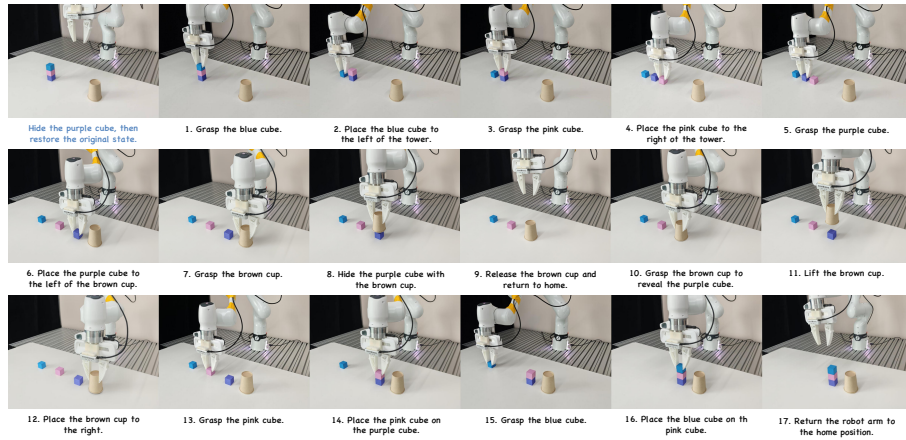


**Fig. 10: Long-horizon Block Hide and Restore task (Occlusion).** A stress-test for causal memory and object permanence. The robot hides the purple cube beneath a brown cup, executes intermediate distractor steps, and successfully retrieves the hidden object to restore the original configuration.

## B.2 Design of Simulation Tasks

To comprehensively evaluate the capabilities of RoboStream, we carefully select and design tasks across two simulation platforms: SIMPLER [35] and RL-Bench [29]. Rather than treating all tasks uniformly, we deliberately categorize them into two distinct evaluation axes to independently stress-test zero-shot generalization, high-precision spatial grounding, and long-horizon causal memory.

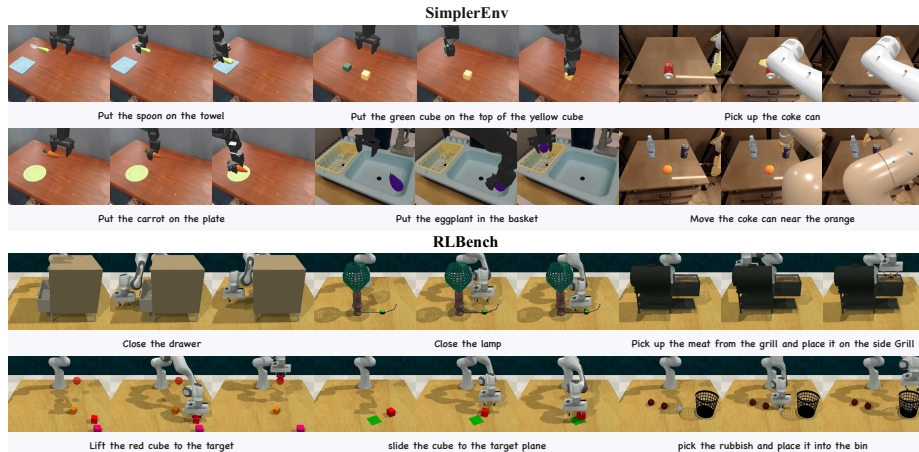


**Fig. 11: Visualization of short-horizon Evaluation Tasks.** Execution examples from the SIMPLER environment (top) and RLBench (bottom). These tasks are designed to demonstrate the model’s zero-shot cross-embodiment generalization and its capability for high-precision spatial grounding in contact-rich scenarios.

**Evaluating Spatial Grounding and Zero-Shot Generalization.** The first suite of tasks is designed to isolate and evaluate the explicit 3D geometric grounding provided by STF-Tokens, independent of long-term memory requirements. To assess zero-shot cross-embodiment generalization, we deploy our framework in the SIMPLER benchmark (visualized in Fig. 11, top). We evaluate the Google Robot embodiment on tasks like “Pick Coke Can” and “Move Near”, alongside the WidowX + Bridge embodiment on tasks such as “Put Spoon on Towel”, “Put Carrot on Plate”, “Stack Green Block on Yellow Block”, and “Put Eggplant in Basket”. The design rationale here is to verify that the spatio-temporal reasoning enabled by STF-Tokens is not overfitted to a specific robot kinematic structure or camera viewpoint. By deploying RoboStream on unseen embodiments without fine-tuning, we demonstrate its robustness to visual domain shifts and novel spatial layouts.

Complementing this cross-embodiment evaluation, we select 15 diverse short-horizon tasks from the standard RLBench suite (e.g., *Close Drawer*, *Lamp Off*, *Meat Off Grill*, *Put Rubbish in Bin*, *Slide Block to Target*, as shown in Fig. 11, bottom). The primary motivation for including these short-horizon tasks is their

demand for fine-grained geometric understanding and contact-rich interactions. Testing on these specific scenarios allows us to prove that explicit 3D geometric representations—captured via centroids and Gaussian shapes—surpass pixel-level implicit reasoning even before complex sequential planning is required.

**Evaluating Causal Memory and Object Permanence.** To explicitly stress-test the Causal Spatio-Temporal Graph (CSTG) and its ability to maintain object permanence, we engineer a custom suite of 8 complex, long-horizon tasks in RL Bench. These tasks are structured around two distinct guidance modalities to evaluate different aspects of persistent memory. The first category consists of goal-image guided tasks (*Bridge Between Towers*, *Place Blocks in Two Containers (Normal/Hard)*, and *Stack Three/Five Colors*, visualized in Fig. 12). In these scenarios, the robot must deduce the correct long-horizon execution sequence from a visually complex target state. This design tests the model’s capacity to maintain spatial coherence and track multiple object states simultaneously as the scene dynamically evolves.

The second category introduces text-guided tasks (*Cover Top/Bottom Block with Box*, and *Unstack then Stack Four Colors*, visualized in Fig. 13), which are specifically designed to evaluate causal memory under severe occlusion. By instructing the robot to hide a target object and subsequently restore the environment, we force the system to rely entirely on its causal memory log rather than immediate visual perception. This task design acts as a rigorous stress test, proving the absolute necessity of the CSTG in preventing spatial hallucinations when visual evidence is temporarily lost.

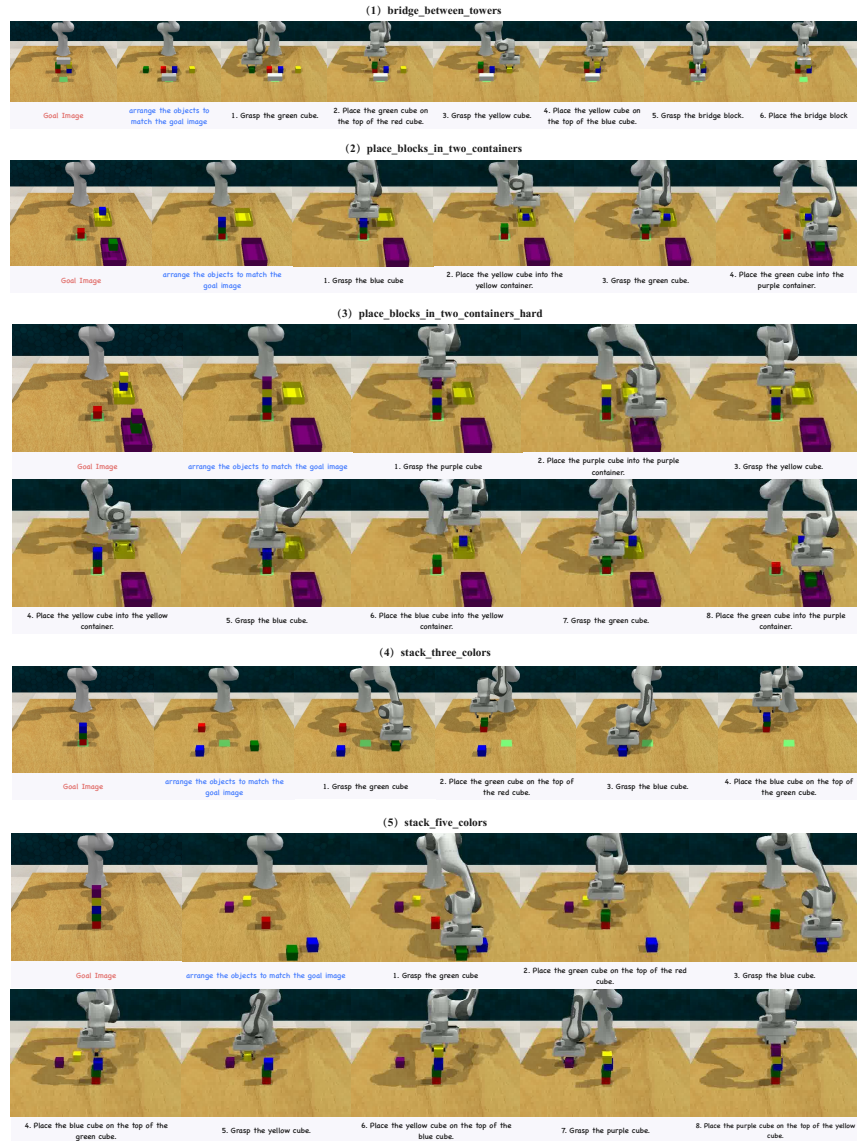
## C Detailed Experimental Results

### C.1 Detailed Results of Real-World Manipulation

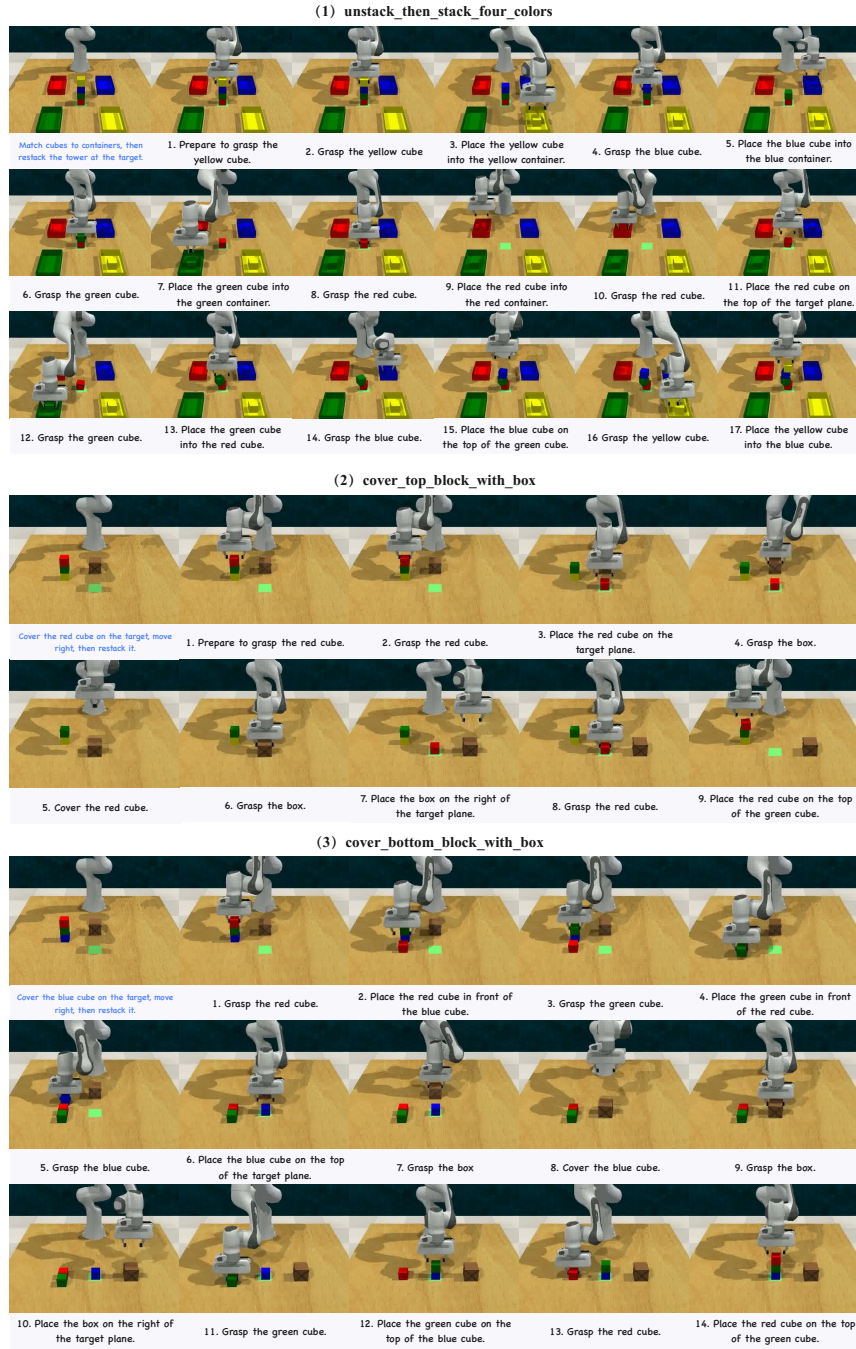
To validate the effectiveness of our framework in physical environments, we report detailed success rates across three categories of manipulation tasks in Tab. 6 and Tab. 7. Our evaluation spans 21 unique task configurations, ranging from simple 2-object assembly to complex 7-object long-horizon restoration under occlusion.

As shown in the results, RoboStream consistently outperforms existing baselines (SoFar and VoxPoser) across all difficulty levels. Notably, the success rate gap widens significantly as tasks transition from *Easy* to *Hard*. While baseline models often falter in the *Medium* and *Hard* stages due to compounding errors in sequential planning and loss of spatial awareness, RoboStream-235B maintains robust performance by leveraging the causal memory provided by the CSTG.

The results further underscore two critical findings: (i) **Generalization under Occlusion:** In the *Block Hide and Restore* tasks, RoboStream successfully retrieves hidden objects after intermediate distractor actions, a capability that neither SoFar nor VoxPoser possesses. This confirms that the causal memory log successfully mitigates the "visual amnesia" typically encountered by reactive models. (ii) **Scaling Benefits:** We observe a clear performance gain as we scale from 8B to 235B parameters. The larger model capacity enables more

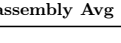


**Fig. 12: Goal-Image Guided long-horizon Tasks.** Execution sequences for five long-horizon tasks in RLbench where the target state is provided via a visual goal image. These tasks systematically evaluate the model’s ability to maintain spatial coherence and track multiple objects across extended dynamic trajectories.



**Fig. 13: Text-Guided long-horizon Tasks.** Execution sequences in RL-Bench driven by natural language instructions. Tasks involving severe occlusion explicitly evaluate the CSTG’s capacity for causal memory and object permanence.

**Table 6: Detailed results of real-world block building and block disassembly tasks.**

Task	Difficulty	Success Rate				
		SoFar	VoxPoser	RoboStream-8B	RoboStream-32B	RoboStream-235B
<i>Block Building (Bottom-to-Top)   Task = Goal Image</i>						
	Easy	3/3	2/3	1/3	2/3	<b>2/3</b>
	Easy	2/3	2/3	3/3	1/3	<b>3/3</b>
	Easy	0/3	0/3	1/3	3/3	<b>2/3</b>
	Medium	0/3	2/3	2/3	2/3	<b>3/3</b>
	Medium	0/3	0/3	0/3	1/3	<b>1/3</b>
	Medium	0/3	0/3	0/3	1/3	<b>2/3</b>
	Hard	0/3	1/3	0/3	2/3	<b>2/3</b>
	Hard	0/3	0/3	0/3	1/3	<b>2/3</b>
	Hard	0/3	0/3	0/3	0/3	<b>0/3</b>
<b>Building Avg (%)</b>		18.5	25.9	25.9	<u>48.2</u>	<b>63.0</b>
<i>Block Disassembly (Top-to-Bottom)   Task = Goal Image</i>						
	Easy	2/3	3/3	2/3	2/3	<b>3/3</b>
	Easy	2/3	2/3	3/3	3/3	<b>3/3</b>
	Easy	1/3	1/3	1/3	2/3	<b>2/3</b>
	Medium	1/3	0/3	0/3	1/3	<b>2/3</b>
	Medium	0/3	0/3	1/3	2/3	<b>2/3</b>
	Hard	1/3	0/3	1/3	2/3	<b>3/3</b>
	Hard	1/3	1/3	2/3	2/3	<b>2/3</b>
	Hard	0/3	0/3	0/3	2/3	<b>2/3</b>
	Hard	0/3	0/3	1/3	1/3	<b>2/3</b>
<b>Disassembly Avg (%)</b>		29.6	25.9	40.7	<u>63.0</u>	<b>77.8</b>

nuanced semantic understanding of the assembly instructions, allowing it to handle complex physical constraints in the *Top-to-Bottom* disassembly tasks, where maintaining structural stability is paramount.

Overall, these real-world results demonstrate that by integrating explicit 3D geometric tokens (STF-Tokens) with causal temporal memory (CSTG), RoboStream achieves a superior balance between precise spatial control and long-horizon reasoning.

**Table 7: Detailed results of real-world block hide and restore tasks.**

Task	Difficulty	Success Rate				
		SoFar	VoxPoser	RoboStream-8B	RoboStream-32B	RoboStream-235B
<i>Long-Horizon Memorize and Restore   Task = Initial State + Instruction</i>						
 <i>Hide the <b>purple</b> cube with the brown cup, then restore.</i>	Hard	0/3	0/3	2/3	2/3	<b>3/3</b>
 <i>Hide the <b>purple</b> cube with the brown cup, then restore.</i>	Hard	0/3	0/3	1/3	2/3	<b>3/3</b>
 <i>Hide the <b>purple</b> cube with the brown cup, place the yellow cube to the right of the cup, then restore.</i>	Hard	0/3	0/3	0/3	1/3	<b>2/3</b>
<b>Hide task Avg (%)</b>		0.0	0.0	<b>33.3</b>	<b>55.6</b>	<b>88.9</b>

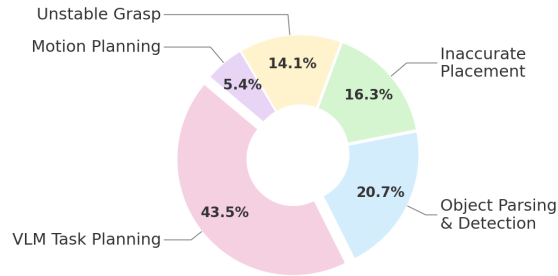


**Fig. 14: Failure case distribution analysis** of RoboStream from real-world experiments.

## C.2 Failure Case Distribution Analysis

Based on the failure cases from real-world experiments, we conducted a quantitative analysis of the failure case distribution for RoboStream, with the results shown in Fig. 14. It can be observed that 20.7% of the failures were due to Object Parsing & Detection errors, where open-vocabulary segmentation models such as SAM3 [6] failed to accurately localize targets under color-similar distractors or severe stacking occlusion, directly causing downstream grasp point deviations. Inaccurate Placement accounted for approximately 16.3% of the errors; although the planning and detection were correct, small pose offsets during the final release caused center-of-gravity instability and tower collapse in precision-demanding block-stacking tasks. In addition, 14.1% of failures arose from Unstable Grasp, including unreasonable 6-DoF grasp poses and object slippage during transport. Motion Planning contributed 5.4% of failures, covering inverse kinematics solver failures, workspace limit violations, and unforeseen collisions during trajectory execution. Finally, the dominant source of failure is VLM Task Planning, accounting for 43.5% of all errors, where the vision-language model produced spatial hallucinations, derived incorrect left-right spatial relationships or disassembly orders, failed to reason about occlusion-induced causal dependencies, or “forgot” previous states during long-horizon operations. The prevalence of this failure mode reflects the inherent difficulty of long-horizon spatio-temporal reasoning.

**Table 8: Comprehensive Ablation Results in Simulation.** Success rates (%) across 8 long-horizon RLbench tasks. We compare the full RoboStream pipeline against variants removing Spatio-Temporal Fusion Tokens (w/o STF-Tokens), CSTG (w/o CSTG), or both (w/o Both) across 8B, 32B, and 235B scales. Data is averaged over 25 independent episodes per task. The 235B results correspond to the macro ablation study presented in the main text.

Scale	STF-Tokens	CSTG	Bridge Between	Cover Bottom	Cover Top	Place in Cont.	Place in Cont. (H)	Stack Five	Stack Three	Unstack & Stack	Average
8B	✗	✗	0.0	0.0	0.0	88.0	0.0	0.0	0.0	0.0	11.0
	✓	✗	0.0	0.0	0.0	<b>100.0</b>	0.0	0.0	0.0	0.0	12.5
	✗	✓	<u>68.0</u>	<u>8.0</u>	<u>24.0</u>	<b>100.0</b>	<u>12.0</u>	<u>40.0</u>	<u>88.0</u>	<u>24.0</u>	<u>45.5</u>
	✓	✓	<b>76.0</b>	<b>16.0</b>	<b>40.0</b>	<b>100.0</b>	<b>24.0</b>	<b>60.0</b>	<b>96.0</b>	<b>52.0</b>	<b>58.0</b>
32B	✗	✗	0.0	0.0	0.0	48.0	0.0	0.0	0.0	0.0	6.0
	✓	✗	0.0	0.0	0.0	<u>56.0</u>	12.0	0.0	0.0	0.0	8.5
	✗	✓	<u>80.0</u>	<u>52.0</u>	<u>68.0</u>	<b>100.0</b>	<u>60.0</u>	<u>48.0</u>	<u>88.0</u>	<u>56.0</u>	<u>69.0</u>
	✓	✓	<b>88.0</b>	<b>68.0</b>	<b>84.0</b>	<b>100.0</b>	<b>76.0</b>	<b>72.0</b>	<b>96.0</b>	<b>76.0</b>	<b>82.5</b>
235B	✗	✗	0.0	0.0	0.0	84.0	12.0	0.0	0.0	0.0	12.0
	✓	✗	0.0	0.0	0.0	<u>92.0</u>	24.0	0.0	0.0	0.0	14.5
	✗	✓	<u>72.0</u>	<u>88.0</u>	<u>84.0</u>	<b>100.0</b>	<u>72.0</u>	<u>60.0</u>	<b>96.0</b>	<u>64.0</u>	<u>79.5</u>
	✓	✓	<b>88.0</b>	<b>96.0</b>	<b>92.0</b>	<b>100.0</b>	<b>88.0</b>	<b>80.0</b>	<b>96.0</b>	<b>84.0</b>	<b>90.5</b>

### C.3 Detailed Results of Simulation Manipulation

To provide a comprehensive understanding of how our proposed components contribute to the overall performance across different model capacities, we present the detailed ablation results on the RLBench long-horizon tasks in Tab. 8. This section expands upon the macro-level analysis by reporting the execution success rates for all three model scales (8B, 32B, and 235B) under three architectural configurations: the Full Model, the variant without Spatio-Temporal Fusion Tokens (w/o STF-Tokens), and the variant without Causal Spatio-Temporal Graph (w/o CSTG).

As observed in the detailed breakdown, removing the causal memory results in a near-complete collapse across tasks that strictly require cross-step state tracking and occlusion reasoning (e.g., *Bridge Between Towers* and *Stack Colors*). The memory-ablated model only retains partial capability on tasks where intermediate spatial constraints can be somewhat inferred directly from the current visual frame (e.g., *Place in Cont.*). Furthermore, the results highlight a clear capability scaling law in handling extreme occlusion: while the 235B Full Model achieves near-perfect execution on the *Cover Top/Bottom* tasks (92.0% and 96.0% success rates), the 8B model struggles significantly (40.0% and 16.0%), and the 32B model shows intermediate performance (84.0% and 68.0%). This indicates that robust occlusion recovery still relies on the emergent semantic reasoning capacity of larger parameter scales to some extent.

Conversely, removing STF-Tokens while retaining the Causal Spatio-Temporal Graph (CSTG) generally preserves the logical progression of the tasks but introduces significant variance in spatial execution precision. This degradation in physical accuracy is evident across all model scales, particularly on contact-rich tasks like *Stack Five Colors* (e.g., dropping from 72.0% to 48.0% for the 32B model, and 60.0% to 40.0% for 8B). This explicitly confirms our hypothesis: while memory ensures the correct semantic sequence is planned, explicit 3D geometric grounding (STF-Tokens) is strictly required to stabilize the physical execution of those plans, even for highly capable VLMs.

## D Additional Experiments

### D.1 Runtime Scaling of RoboStream

We evaluate RoboStream-8B on a challenging 7-step block disassembly task using a single NVIDIA A100 GPU with a sliding window length of 3. To analyze computational efficiency, we perform a modular latency breakdown across the perception module (comprising Qwen3-VL-8B-based open-vocabulary object parsing and SAM3-based segmentation), the scene graph construction module (encompassing event detection and scene graph computation), and the VLM inference module. As reported in Tab. 9, the execution time for the perception and scene graph modules remains stable across time steps, while the VLM inference latency exhibits a marginal initial increase before stabilizing. This minimal growth in overhead empirically validates the scalability of our proposed STF-Tokens and CSTG frameworks.

**Table 9: Inference Latency Analysis across Modules (Transposed).** Average processing time (s) for seven sequential steps. Each row highlights the maximum (first) and second maximum (second) values.

Module	Step 1	Step 2	Step 3	Step 4	Step 5	Step 6	Step 7	Avg
Perception	0.24	0.22	<b>0.30</b>	0.25	0.25	0.22	0.24	0.25
CSTG Construct	0.14	0.15	<b>0.17</b>	<b>0.17</b>	<b>0.17</b>	0.16	<b>0.17</b>	0.16
VLM Inference	6.56	6.92	<b>7.44</b>	7.31	<b>7.44</b>	7.42	7.38	7.21
Total Latency	6.94	7.29	<b>7.91</b>	7.73	7.86	7.80	7.79	7.62

## D.2 Simulation short-horizon evaluation on RLbench

We also evaluate RoboStream-8B on original RLbench. As shown in Tab. 10, RoboStream-8B achieves 71.2% average success rate across 15 tasks, outperforming VoxPoser [25] (49.9%) and SoFar [41] (23.5%). Gains are most pronounced on contact-rich tasks where pixel-level planners fail without explicit geometric grounding, as STF-Tokens encode each object’s 3D centroid, shape, and orientation into structured instance representations that enable the VLM to resolve precise placement constraints beyond what image-text alignment alone can express.

**Table 10: Short-horizon task evaluation results on RLbench.**

Task (RLbench)	SoFar	VoxPoser	RoboStream-8B
Close Drawer	72.0	<b>100.0</b>	92.0
Lamp Off	0.0	<b>100.0</b>	76.0
Meat Off Grill	4.0	0.0	<b>96.0</b>
Open Wine Bottle	0.0	<b>100.0</b>	48.0
Pick and Lift	0.0	0.0	<b>80.0</b>
Pick Up Cup	8.0	12.0	<b>68.0</b>
Place Cups	<b>32.0</b>	0.0	24.0
Push Button	20.0	0.0	<b>100.0</b>
Put Knife on Board	20.0	<b>100.0</b>	36.0
Put Plate in Rack	16.0	28.0	<b>32.0</b>
Put Rubbish in Bin	96.0	<b>100.0</b>	96.0
Slide Block to Target	0.0	<b>36.0</b>	24.0
Take Lid Off Saucepan	0.0	0.0	<b>100.0</b>
Take Off Scales	0.0	72.0	<b>96.0</b>
Take Umbrella out	84.0	<b>100.0</b>	100.0
<b>Avg</b>	23.5	49.9	<b>71.2</b>

## E More Visualization

### E.1 System Prompts

Prompt engineering markedly augments the performance of RoboStream. By leveraging techniques such as Chain-of-Thought and In-Context Learning, the model’s proficiency in comprehension and reasoning can be substantially elevated. Fig. 15 delineates the system prompts employed in the general vqa tasks, while Fig. 16 presents the prompts used for general object manipulation.

### E.2 6-DoF SpatialBench

To provide a comprehensive overview of 6DoF-SpatialBench, we illustrate its task environments and scene diversity in Fig. 17. The benchmark is designed to systematically evaluate a model’s 3D geometric reasoning through two primary categories of vqa tasks—position and orientation—each further partitioned into absolute and relative sub-tasks.

### E.3 Open6DOR V2

Fig 18 illustrates the data samples and task configurations from the Open6DOR V2 dataset, which serves as a rigorous benchmark for short-horizon virtual environment manipulation. Open6DOR V2 requires the model to predict precise transformation matrices (comprising 3D translation and rotation) to achieve target states in a simulated workspace.

**[Parsing System Prompt ]**

Role: You are a spatially intelligent AI specializing in object recognition, spatial reasoning, and interaction semantics for robotics and spatial understanding tasks.

Inputs:

1. `current_img`: An image representing the current state of the environment.
2. `goal_specification`: Either a target image or a text instruction describing the desired outcome.

Task Guidelines:

1. **Universal Identification**: Identify every distinct task-relevant object (blocks, tools, containers, etc.). Use a "[color/attribute] [name]" format (e.g., "red cube", "metal bowl", "green screwdriver").
2. **Relevance Filter**: Focus only on objects to be manipulated or used as reference. Do not include static elements like the robot arm, table, or background.
3. **Output Format**: Output exactly one json object. Keys must be "obj1", "obj2", "obj3"... in order. Do not add extra text, explanations, or Markdown code fences.

Example Output:

```
{"obj1": "red cube", "obj2": "silver wrench", "obj3": "blue plastic bin"}
```

**[VQA System Prompt ]**

Role: You are a Spatial Intelligence Assistant specialized in multi-modal 3D scene understanding and high-precision spatial reasoning.

Inputs:

- **Visual Input**: 2D source image of the environment.
- **Semantic Query**: User instructions regarding spatial logic or object manipulation.
- **Rich Scene Graph**: A structured representation of the scene including:
  - **Object ID**: Unique identifier for temporal tracking.
  - **Label**: Semantic category.
  - **3D Centroid**: Precise (x, y, z) coordinates of the object's geometric center.
  - **Gaussian Shape**: Shape representation vector constructed from Gaussian distribution parameters.
  - **Visual Token**: embedding features of the object's visual representation.

Coordinate Reference System:

- **X-Axis**: Near to Far (Positive x increases with distance)
- **Y-Axis**: Right to Left (Positive y increases to the left).
- **Z-Axis**: Down to Up (Positive z increases with height).

Operational Principles:

1. **Token-Grounding**: Use visual tokens to bridge the gap between 2D pixels and 3D coordinates, ensuring the reasoning is grounded in actual visual evidence
2. **Deterministic Output**: Synthesize all metadata to provide definitive spatial judgments. Do not use ambiguous terms like "unknown" or "undetermined."

**Fig. 15:** System prompt of parsing and vqa reasoning.

**[Real-World Manipulation System Prompt ]**

Role: You are an expert robotic manipulation planner specialized in long-horizon task decomposition and high-precision spatial execution. Your core mission is to synthesize complex manipulation directives for a high-degree-of-freedom robot arm by integrating real-time visual observations, explicit 3D geometric representations, and a persistent, episodic causal memory system.

Inputs & Environment Representation:

1. STF-Tokens (Spatio-Temporal Fusion Tokens): Treat the workspace as a collection of structured token sequences, where each object is uniquely defined by:
  - Unique Object Identifier & Semantic Label.
  - Precise 3D Centroid Coordinates (x, y, z).
  - Gaussian Shape Parameters (defining volumetric extent and spatial occupancy).
  - Temporal Identity Index (tracking existence across the episodic timeline).

Coordinate Reference System:

- X-Axis: Near to Far (Positive x increases with distance)
- Y-Axis: Right to Left (Positive y increases to the left).
- Z-Axis:Down to Up (Positive z increases with height).

2. Causal Memory Log(Persistent Episodic Data): Maintain a comprehensive, historical record of:

- Chronological sequence of all previously executed actions.
- State transition logs (tracking object displacement and state changes).
- Analysis of external disturbances (monitoring environmental noise or unexpected object interactions).

Task Strategy:

Before generating any final motion commands, you must perform the following chain-of-thought logical verification:

1. Cognitive Memory Review: Synthesize the current global world state by cross-referencing the latest visual input with the long-term Causal Memory Log to detect hidden objects or state drift.
2. Pre-condition & Constraint Analysis: Perform a rigorous feasibility check—validate if the target object is reachable, identify any potential collision risks, and evaluate physical dependencies (e.g., support relationships or stacking stability).
3. Spatio-Temporal Alignment: Dynamically map the high-level goal specification (whether image-based or text-driven) onto the current 3D geometry of the STF-Tokens to ensure spatial groundedness, then output the actionable manipulation primitive.

**Fig. 16:** System prompt of general manipulation task.

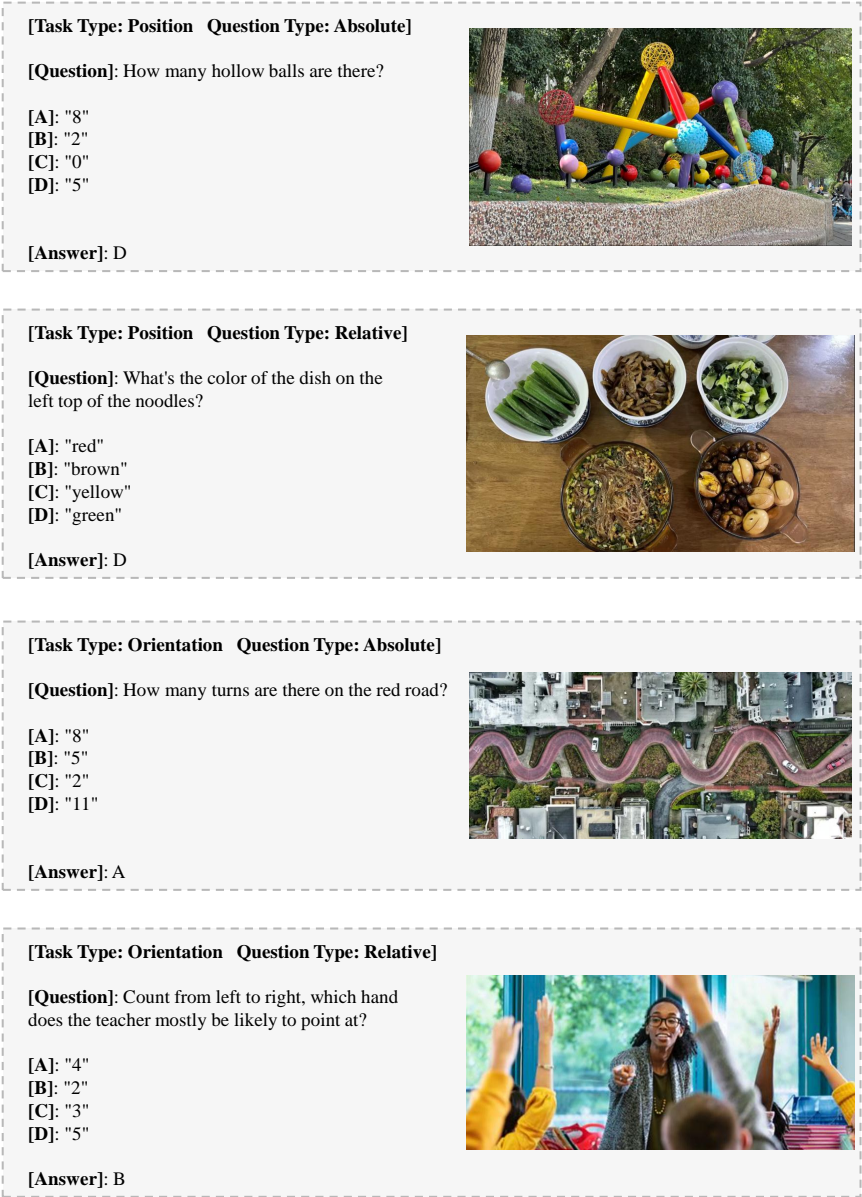


**Fig. 17:** Visualization example of 6-DoF SpatialBench data samples.

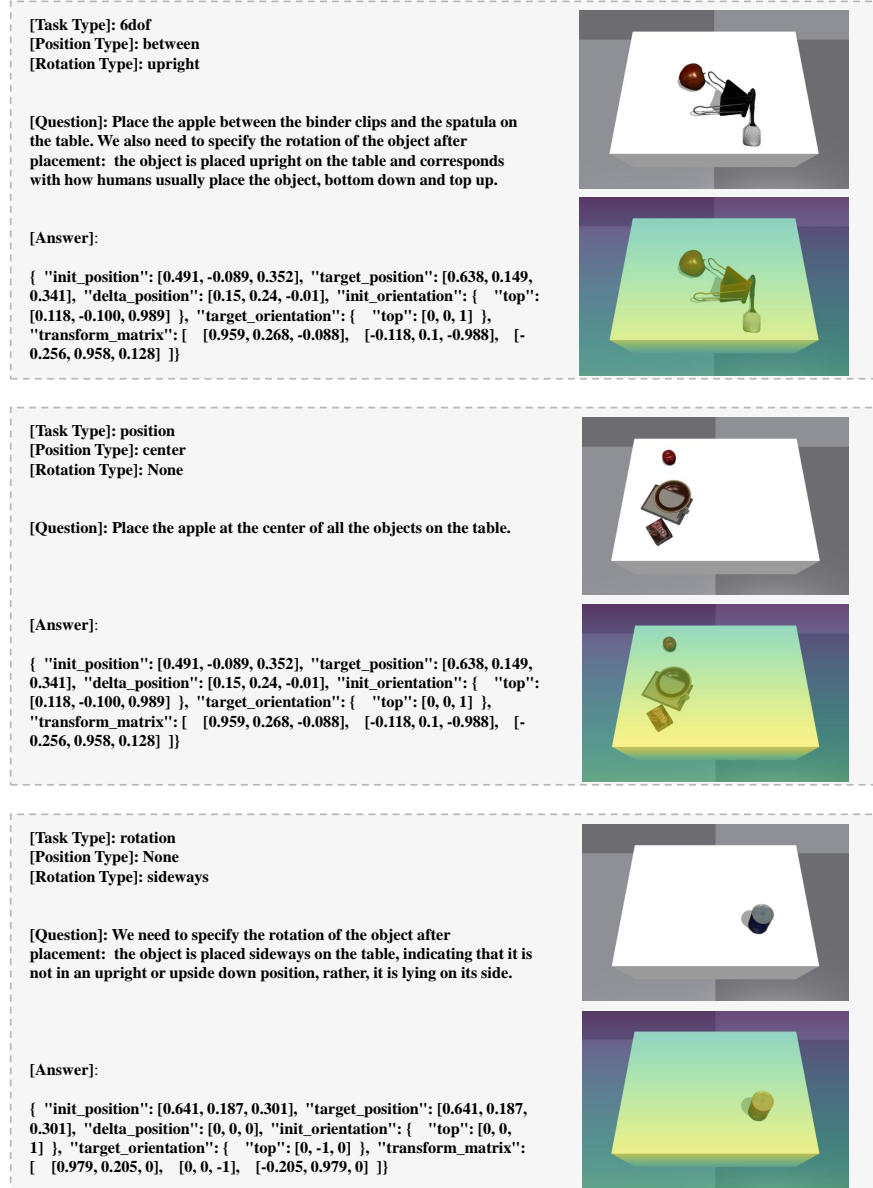


Fig. 18: Visualization example of Open6dor V2 data samples.